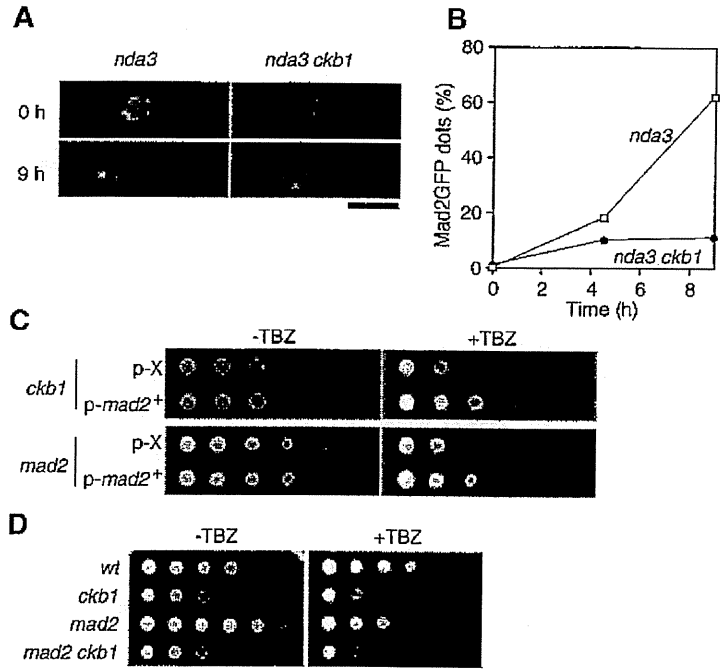

Fig. 2. CK2 is required for the localization of Mad2p at unattached kinetochores. (A, B) Cells (*nda3*, HM5170; *nda3 ckb1*, HM5741) were grown exponentially in EMM2 medium at 34 °C. (A) At time 0, the temperature was shifted to 18 °C, Mad2-GFP was visualized at the indicated times. Bar, 5 μm. (B) The percentage of cells with Mad2-GFP dots was determined. (C) Exponentially growing cells (*ckb1*, HM3584; *mad2*, HM1338) harboring pREP81-*mad2*$^+$ (p-*mad2*$^+$) or an empty vector (p-*x*) were spotted onto EMM plates without (−TBZ) or with 0.015 mg/ml TBZ (+TBZ). Plates were incubated at 32 °C for *ckb1* and at 30 °C for *mad2* for 3 days. (D) Exponentially growing cells (*wt*, HM4; *ckb1*, HM3584; *mad2*, HM1338; *mad2 ckb1*, HM5177) were spotted onto YES plates without (−TBZ) or with 0.015 mg/ml TBZ (+TBZ). Plates were incubated at 30 °C for 2 days.

expression of *mad2*$^+$ indeed restored viability to *ckb1*-deleted cells, as also observed for *mad2*-deleted cells after TBZ treatment. We thus concluded that *mad2*$^+$ functions downstream of *ckb1*$^+$.

To clarify the relative contributions of *ckb1*$^+$ and *mad2*$^+$ to the regulation of the SAC, we constructed a *mad2 ckb1* double mutant and monitored its viability after exposure to TBZ (Fig. 2D). The viability of *mad2 ckb1* cells was similar to that of the *ckb1* mutant, suggesting that *ckb1*$^+$ and *mad2*$^+$ act in the same pathway.

We next examined the effects of TBZ exposure on the abundance of Mad2p in CK2 mutants (Fig. 3A and B). The amount of Mad2p in *wt* cells did not vary after treatment of exponential cultures with TBZ at either 32 °C or 20 °C. In contrast, the amount of Mad2p in *ckb1* cells was low in the presence or absence of TBZ (Fig. 3A). The amount of Mad2p increased after heat shock treatment, whereas this increase was not observed in *orb5* cells (Fig. 3B). These results suggest that CK2 is partially required for the maintenance of Mad2p independent of the SAC activation. It is possible that in *ckb1* cells failure of the localization of Mad2-GFP to unattached kinetochores is due to the low protein level of Mad2p. However, it is unlikely since Mad2-GFP was detected in the nuclear periphery and chromatin domain in *ckb1* cells.

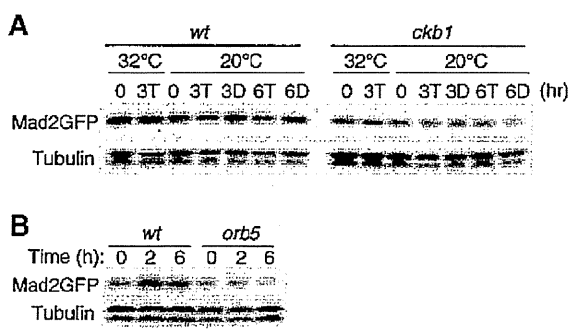

Fig. 3. The Mad2p level is low in CK2 mutants. (A) *wt* (HM5170) and *ckb1* (HM5172) cells were grown to mid-log phase in YES medium at 32 °C (32 °C, 0). TBZ (0.1 mg/ml) was added at time 0 and samples were collected after 3 h (32 °C, 3T). After the cells were grown at 32 °C, the temperature was shifted to 18 °C in YES medium without (D) or with TBZ (T). Samples were collected at the indicated times and subjected to immunoblot analysis using an anti-GFP antibody. (B) *wt* (HM5170) and *orb5* (HM5265) cells were grown to mid-log phase in YES medium at 24 °C. The temperature was shifted to 36 °C at time 0. Samples were analyzed as in (A).

We next tested whether protein levels and localization of Orb5p and Ckb1p change in response to activation of the SAC. The protein level did not vary with TBZ treatment (Supplementary figure 1). However, the levels of both proteins increased in *nda3* mutant cells compared with *wt* cells, but these levels did not change after the temperature shift. This result may reflect the fact that Orb5p and Ckb1p did not vary in response to SAC activation, but due to other defects in *nda3* cells. We found that Orb5p and Ckb1p were constitutively present in the nucleus with and without the activation of the SAC (Supplementary figure 2). In higher eukaryotes, CK2 is associated with centromeres and the mitotic spindle during mitosis [21]. It is likely that a sub-fraction of fission yeast CK2 is associated with the kinetochores, where it might regulate the localization of Mad2p when the SAC is activated.

We have shown that *ckb1* and *orb5* mutants exhibit the defining feature of a metaphase checkpoint defect — the failure to arrest in metaphase in the presence of spindle damage. In addition, these mutants show sensitivity to the microtubule-destabilizing drug TBZ. We have also found that Ckb1p is required for the localization of Mad2p to unattached kinetochores. In all of these respects, *ckb1* and *orb5* mutant phenotypes are qualitatively similar to those described for perturbations of the classical checkpoint components Mad1p and Mad2p. However, in *ckb1* and *orb5* mutants the protein

level of Mad2p is low. These facts suggest that CK2 is required for the SAC both directly and indirectly. It has been shown that human CK2 is involved in mitotic arrest following spindle damage [22]. We propose that CK2 represents additional components or regulators of the metaphase checkpoint that have been conserved among eukaryotes.

Loss of mitotic checkpoint control is a common event in human cancer cells, which is thought to be responsible for their frequently observed chromosome instability, although many cancer-derived samples do not contain mutations in SAC proteins [23]. The molecular nature of the defect underlying the absence of the SAC in most of these cell lines is not known [24]. Recent studies have shown that reduced levels of Mad2 expression can be detected in nasopharyngeal carcinoma, ovarian cancer and breast cancer cell lines and ovarian cancer [25,26]. Complete loss of Mad2p in various results in embryonic lethality owing to chromosome mis-segregation [27]. It is likely that partial loss of the SAC leads to tumor development in cells that are undergoing tumorigenesis. We have shown that the Mad2p level is decreased in CK2 mutants in fission yeast. Since CK2 is highly conserved among eukaryotes, it is possible that tumor cells harboring a SAC defect have CK2 mutations.

In conclusion, we have shown that CK2 plays an essential role on the SAC that has been conserved among eukaryotes. The molecular mechanism how CK2 regulates Mad2p remains to be determined. Future studies should provide invaluable insights into understanding the role of CK2 in the SAC.

Acknowledgments

We thank P. Nurse and T. Toda for yeast strains and K. Okazaki for plasmids and helpful discussion. This work was supported in part by a grant-in-aid for Scientific Research from the Ministry of Education, Culture, Sports, Science, and Technology of Japan (to H.M. and Y.M-T.).

Appendix A. Supplementary data

Supplementary data associated with this article can be found, in the online version, at doi:10.1016/j.bbrc.2009.08.030.

References

[1] D.W. Cleveland, Y. Mao, K.F. Sullivan, Centromeres and kinetochores: from epigenetics to mitotic checkpoint signaling, Cell 112 (2003) 407–421.
[2] S. Hauf, Y. Watanabe, Kinetochore orientation in mitosis and meiosis, Cell 119 (2004) 317–327.
[3] H. Murakami, P. Nurse, DNA replication and damage checkpoints and meiotic cell cycle controls in the fission and budding yeasts, Biochem. J. 349 (2000) 1–12.
[4] A. Musacchio, E.D. Salmon, The spindle-assembly checkpoint in space and time, Nat. Rev. Mol. Cell Biol. 8 (2007) 379–393.
[5] L.J. Vos, J.K. Famulski, G.K. Chan, How to build a centromere: from centromeric and pericentromeric chromatin to kinetochore assembly, Biochem. Cell Biol. 84 (2006) 619–639.
[6] G.K. Chan, S.T. Liu, T.J. Yen, Kinetochore structure and function, Trends Cell Biol. 15 (2005) 589–598.
[7] R. Karess, Rod-Zw10-Zwilch: a key player in the spindle checkpoint, Trends Cell Biol. 15 (2005) 386–392.
[8] E. Montembault, S. Dutertre, C. Prigent, R. Giet, PRP4 is a spindle assembly checkpoint protein required for MPS1, MAD1, and MAD2 localization to the kinetochores, J. Cell Biol. 179 (2007) 601–609.
[9] M. Yanagida, Cell cycle mechanisms of sister chromatid separation; Roles of Cut1/separin and Cut2/securin, Genes Cells 5 (2000) 1–8.
[10] J.M. Peters, The anaphase-promoting complex: proteolysis in mitosis and beyond, Mol. Cell 9 (2002) 931–943.
[11] A.E. Ikui, K. Furuya, M. Yanagida, T. Matsumoto, Control of localization of a spindle checkpoint protein, Mad2, in fission yeast, J. Cell Sci. 115 (2002) 1603–1610.
[12] M. Shimada, C. Namikawa-Yamada, M. Nakanishi, H. Murakami, Regulation of Cdc2p and Cdc13p is required for cell cycle arrest induced by defective RNA splicing in fission yeast, J. Biol. Chem. 280 (2005) 32640–32648.
[13] I. Sugimoto, H. Murakami, Y. Tonami, A. Moriyama, M. Nakanishi, DNA replication checkpoint control mediated by the spindle checkpoint protein Mad2p in fission yeast, J. Biol. Chem. 279 (2004) 47372–47378.
[14] F. Meggio, L.A. Pinna, One-thousand-and-one substrates of protein kinase CK2?, FASEB J 17 (2003) 349–368.
[15] I. Roussou, G. Draetta, The *Schizosaccharomyces pombe* casein kinase II alpha and beta subunits: evolutionary conservation and positive role of the beta subunit, Mol. Cell Biol. 14 (1994) 576–586.
[16] S. Moreno, A. Klar, P. Nurse, Molecular genetic analysis of fission yeast *Schizosaccharomyces pombe*, Methods Enzymol. 194 (1991) 795–823.
[17] J. Bahler, J.Q. Wu, M.S. Longtine, N.G. Shah, A. McKenzie 3rd, A.B. Steever, A. Wach, P. Philippsen, J.R. Pringle, Heterologous modules for efficient and versatile PCR-based gene targeting in *Schizosaccharomyces pombe*, Yeast 14 (1998) 943–951.
[18] K. Okazaki, N. Okazaki, K. Kume, S. Jinno, K. Tanaka, H. Okayama, High-frequency transformation method and library transducing vectors for cloning mammalian cDNAs by trans-complementation of *Schizosaccharomyces pombe*, Nucleic Acids Res. 18 (1990) 6485–6489.
[19] H. Murakami, P. Nurse, Meiotic DNA replication checkpoint control in fission yeast, Genes Dev. 13 (1999) 2581–2593.
[20] T. Toda, K. Umesono, A. Hirata, M. Yanagida, Cold-sensitive nuclear division arrest mutants of the fission yeast *Schizosaccharomyces pombe*, J. Mol. Biol. 168 (1983) 251–270.
[21] W. Krek, G. Maridor, E.A. Nigg, Casein kinase II is a predominantly nuclear enzyme, J. Cell Biol. 116 (1992) 43–55.
[22] M. Sayed, S. Pelech, C. Wong, A. Marotta, B. Salh, Protein kinase CK2 is involved in G2 arrest and apoptosis following spindle damage in epithelial cells, Oncogene 20 (2001) 6994–7005.
[23] C.S. Lopes, C.E. Sunkel, The spindle checkpoint: from normal cell division to tumorigenesis, Arch. Med. Res. 34 (2003) 155–165.
[24] T. Takahashi, N. Haruki, S. Nomoto, A. Masuda, S. Saji, H. Osada, T. Takahashi, Identification of frequent impairment of the mitotic checkpoint and molecular analysis of the mitotic checkpoint genes, hsMAD2 and p55CDC, in human lung cancers, Oncogene 18 (1999) 4295–4300.
[25] X. Wang, D.Y. Jin, Y.C. Wong, A.L. Cheung, A.C. Chun, A.K. Lo, Y. Liu, S.W. Tsao, Correlation of defective mitotic checkpoint with aberrantly reduced expression of MAD2 protein in nasopharyngeal carcinoma cells, Carcinogenesis 21 (2000) 2293–2297.
[26] M.J. Percy, K.A. Myrie, C.K. Neeley, J.N. Azim, S.P. Ethier, E.M. Petty, Expression and mutational analyses of the human MAD2L1 gene in breast cancer cells, Genes Chromosomes Cancer 29 (2000) 356–362.
[27] L.S. Michel, V. Liberal, A. Chatterjee, R. Kirchwegger, B. Pasche, W. Gerald, M. Dobles, P.K. Sorger, V.V. Murty, R. Benezra, MAD2 haplo-insufficiency causes premature anaphase and chromosome instability in mammalian cells, Nature 409 (2001) 355–359.

Biochemical and Biophysical Research Communications 380 (2009) 460–466

Contents lists available at ScienceDirect

Biochemical and Biophysical Research Communications

journal homepage: www.elsevier.com/locate/ybbrc

Ptpcd-1 is a novel cell cycle related phosphatase that regulates centriole duplication and cytokinesis

Doaa H. Zineldeen, Midori Shimada, Hiroyuki Niida, Yuko Katsuno, Makoto Nakanishi *

Department of Cell Biology and Biochemistry, Graduate School of Medical Sciences, Nagoya City University, 1 Kawasumi, Mizuho-cho, Mizuho-ku, Nagoya 467-8601, Japan

ARTICLE INFO

Article history:
Received 6 January 2009
Available online 24 January 2009

Keywords:
Centrosome
Phosphatase
Mitosis
Polo-like kinases
Cytokinesis
Cdc14

ABSTRACT

Proper progression of mitosis requires spatio-temporal regulation of protein phosphorylation by orchestrated activities of kinases and phosphatases. Although many kinases, such as Aurora kinases, polo-like kinases (Plks), and cyclin B-Cdk1 are relatively well characterized in the context of their physiological functions at mitosis and regulation of their enzymatic activities during mitotic progression, phosphatases involved are largely unknown. Here we identified a novel protein tyrosine phosphatase containing domain 1 (Ptpcd 1) as a mitotic phosphatase, which shares sequence homology to Cdc14. Immunofluorescence studies revealed that Ptpcd1 partially colocalized with γ-tubulin, an archetypical centrosomal marker. Overexpression of this phosphatase prevented unscheduled centrosomal amplification in hydroxyurea arrested U2OS cells. Intriguingly, Ptpcd 1-associated and colocalized with polo-like kinase 1(Plk1). Hence, overexpression of Ptpcd1 rescued prometaphase arrest of Plk-1 depleted cells, but resulted in aberrant cytokinesis as did as Plk1 overexpression. These results suggested that Ptpcd1 is involved in centrosomal duplication and cytokinesis.

© 2009 Elsevier Inc. All rights reserved.

Faithful transmission of genetic information relies on the coordinated regulatory system of the cell cycle [1]. In higher eukaryotes, mitosis involves many dynamic processes at chromosomes, including condensation and segregation, both of which are mainly regulated by protein phosphorylation and dephosphorylation [2]. Proper segregation of chromosomes requires centrosomal maturation, separation, spindle formation and alignment of chromosomes [2,3]. Centrosome is the major microtubule organizing center in animal cells composed of two centrioles, which are barrel shaped structures with nine triple microtubules and a pericentriolar matrix responsible for nucleating microtubules and organizing mitotic spindles for bipolar separation of sister chromatids [4,5]. The identification of several centrosome-associated protein kinases has proposed the concept that multiple regulatory phosphorylation pathways tightly control centrosome cycle during cell cycle [6–8]. Around G1/S transition, a procentriole forms adjacent to each parental centriole and continues growing during S phase. At the onset of mitosis, the two centrosomes separate and the daughter centriole matures and instructs mitotic spindle formation [4]. In post-mitotic cells, centrosome migrates to the cell surface and one of the centrioles differentiates into a basal body that nucleates microtubules to form a cilium [5].

Polo-like kinases (Plks) regulate a multitude of several mitotic processes, including centrosome duplication, maturation [9], bipolar spindle formation [10], microtubule/kinetochore interactions, and cytokinesis [11,12]. Spatio-temporal coordination of Plks activities is achieved through binding to phosphorylated docking proteins with distinct subcellular localizations, such as centrosomes, kinetochore, and the midzone [12,13]. At early mitosis, Cdk1 creates the phosphorylated docking sites on the substrates [1], whereas Plks create their own docking sites on other partners after inactivation of Cdk1 [1,12,13]. In budding yeast, some parts of mitotic function of Plks appear to be mediated by Cdc14p. Cells lacking Cdc14p are unable to exit from mitosis, with defects in both movement of chromosomes to the spindle poles and elongation of anaphase spindles [14]. Mammalian cells possess two Cdc14 paralogue, Cdc14A and Cdc14B, identified based on their sequence similarity to Cdc14p [15]. Recent studies suggested that Cdc14A and Cdc14B might be involved in distinctive cellular functions; the former functioned in centrosomal separation and cytokinesis [3,16], and the latter in centrosomal duplication and microtubule stabilization [17]. However, Cdc14B deficient cells were viable and lacked apparent defects in chromosome segregation and cytokinesis [18], suggesting that alternative phosphatase(s) might be capable of complementing the mitotic functions of Cdc14B. Here, we identified Ptpcd1 as a possible functional isozyme of mammalian Cdc14B that is genetically linked to Plk1.

Materials and methods

Cloning of Ptpcd1. The complete ORF of Ptpcd1 (corresponding exactly to AW456874; No. NM 207232 and MGI: 2145430) was

* Corresponding author. Fax: +81 52 842 3955.
E-mail address: mkt-naka@med.nagoya-cu.ac.jp (M. Nakanishi).

0006-291X/$ - see front matter © 2009 Elsevier Inc. All rights reserved.
doi:10.1016/j.bbrc.2009.01.113

amplified by PCR using mouse brain cDNA library as a template with the following primer set: 5′-ATG GCG CAG GAG TCT TGC CA-3′ and 5′-TCA GGA GAG GCT GCT GTC CTT TTT GC-3′. The PCR product was subcloned into pCR II-TOPO (Invitrogen). pcDNA3.1-Myc/HisPtpcd1 was then generated by subcloning of the KpnI/NotI fragment into pcDNA3.1Myc/His vector. The KpnI/NotI fragment was amplified by PCR using pCRII-TOPOPtpcd1 as a template with a set of primers; 5′-TTT GAA TTC GCC ACC ATG TCG TCC GGG GCC AAG GAG-3′and 5′-AAA TCT AGA GGG CAG AGG GGT CCC GTT-3′. pcDNA3.1Plk1-HA was generated by subcloning of EcoRI/NotI fragment from pET23d-Plk1 (kind gift from Dr. Nishida) into pcDNA3.1HA.

Cell culture. HeLa and U2OS cells were cultured and maintained in Dulbecco's modified Eagle's medium (Invitrogen) supplemented with 10% fetal bovine serum as described previously [19]. Nocodazole and hydroxyurea were purchased from Sigma.

Knockdown experiments. Plasmid transfections were performed using FuGENE6 transfection reagent (Roch) according to manufacturer's instruction. Stealth siRNAs for Plk1 (Invitrogen) or control (Invitrogen) were transfected using lipofectamin 2000 (Invitrogen).

Immunoblotting. Antibodies used in this study were anti-c-myc (sc-789; Santa Cruz, sc-40; Santa Cruz), anti-pTyr-Cdk1 (9111; Cell signaling), anti-cyclin B1 (GNS1; Santa Cruz), anti-Plk1 (35-200; upstate), anti-HA (12CA5; Roch), anti-γ-tubulin (T3559; Sigma) and anti-α-tubulin (Sigma). Whole cell extracts were prepared as described previously [20] and were subjected to immunoblotting. For IP-immunoblotting, U2OS cells were cotransfected with Plk1-HA, along with Ptpcd1-myc or empty pcDNA3.1. Cells were harvested in RIPA buffer (10 mM Tris–HCl, pH7.5, 150 mM NaCl, 0.5% Triton X-100, 1% sodium deoxycholate and complete protease inhibitor tablets (1/10 ml) (Roch). The lysates (200 μg) were incubated with anti-myc antibodies (5 μg) or mouse normal IgG as a control at 4 °C for 1 h and then precipitated with 20 μl of protein G beads. The resultant precipitates were separated by SDS–PAGE and then analyzed by immunoblotting.

Microtubule regrowth assay. Cells on coverslips were treated with 4 mM nocodazole for 30 min at 37 °C, followed by replacement with normal medium. Cells were fixed at −20 °C with methanol and immunostained for immunofluorescence microscopy was performed as described previously [21].

Immunofluorescence analysis. Secondary antibodies for immunofluorescence microscopy were Cy3 (Jackson immunoresearch), Alexa 594 and Alexa 488 (Molecular probes). Cells on coverslips were fixed in 4% PFA for 10 min at RT and then permeabilized with 0.25% Triton X-100 in PBS. Blocking was done in 5% normal goat serum (Convac) containing 1% Triton X-100. Fixed cells were incubated with antibodies in blocking for 1 h at RT. DNA was counterstained with DAPI (2 mg/ml). For centrosomal staining, cells were fixed with methanol at −20 °C for 10 min.

Results and discussion

Ptpcd 1 is a centrosomal phosphatase that regulates centrosomal duplication during S phase

Immotile primary cilium is a centriole-based organelle that consists of microtubule pairs located at the plasma membrane [22]. The fact that a cilium is differentiated from centrosomes after mitosis has suggested that the function and structures of cilia are regulated by similar mechanisms to those of centrosomes [23]. Indeed, Nek2 and Aurora A kinases are involved in the regulation of both centrosomes and cilia functions [24]. Ptpcd 1 was originally identified as a dual specificity protein phosphatase highly expressed in mouse cilia [25]. We therefore speculated that Ptpcd 1 might be involved in the regulation of centrosomal function. Ptpcd 1 encodes a 721 amino acid protein with a predicated molecular weight of 82 kDa. Sequence analysis of Ptpcd1 revealed the significant homology with yeast Cdc14p with coiled coil domain at its carboxyl terminal, RXXL motif (a putative APC/C binding motif), several nuclear localization signals (Suppl. Fig. 1A), and a putative nuclear export signal (Suppl. Fig. 1B). To examine whether Ptpcd1 functions at centrosomes, Ptpcd1-myc was transfected into HeLa cells. In interphase cells, signals corresponding to Ptpcd1 were detected at both cytoplasm and nucleus with one or two closely spaced dots. Importantly, these dot signals were localized adjacent to, but not overlapped with, the signals from γ-tubulin, a centrosomal protein, raising the possibility of its centriolar localization (Fig. 1A). This centrosomal enrichment of Ptpcd1 was observed from interphase to anaphase, whereas it was hardly detected at telophase where most of the immunoreactivity was detected at midbody. This spatio-temporal localization in relation to cell cycle conveyed that Ptpcd1 might be a novel centrosomal-related phosphatase.

In certain transformed cells, such as U2OS cells, prolonged S phase arrest by hydroxyurea (HU) causes uncoupled centrosomal duplication from cell cycle with multiple rounds of centriole duplication in the absence of DNA replication and mitotic division (Fig. 1B, upper panel) [15]. In order to examine whether Ptpcd-1 plays a role in the regulation of centriole duplication, Ptpcd1 were overexpressed into U2OS cells in the presence of 4 mM HU for 72 h. Ptpcd 1 expression inhibited HU-induced centriole over duplication (Fig. 1B, lower panel). Majority of control U2OS cells possessed more than single centrosome when cells were treated with HU. In contrast, 60% of Ptpcd 1 expressing cells possessed single centrosome (Fig. 1C). These results clearly indicated that overexpression of Ptpcd1 suppressed uncoupled centrosomal duplication during S phase. Given that Cdk activity regulates centrosomal duplication during S phase, we asked whether Ptpcd1 affect inhibitory phosphorylation of Cdc2 at Y15, which is regulated at centrosomes during S to G2 phase. Cdc2 phosphorylation at Y15 slightly decreased, whereas expression of cyclin B1 was not affected by Ptpcd1 expression (Fig. 1D).

Ptpcd1 associates with Plk1 and is involved in the regulation of mitotic progression

Plk1 regulates centrosomal functions at multiple levels, such as centrosomal stabilization, nucleation, duplication, microtubule stabilization, and cytokinesis [9–13]. Therefore, Ptpcd1 might be involved in Plk1-dependent regulation of centrosome functions. To examine this possibility, we first asked whether Ptpcd1 physically interact with Plk1. Plk1-HA and Ptpcd1-myc were co-transfected into HeLa cells and the cell extracts were immunoprecipitated with anti-myc antibodies. Plk1-HA as well as Ptpcd1-myc was readily detected in the myc-immunoprecipitates, indicating that Plk1-HA was capable of forming a complex with Ptpcd1-myc (Fig. 2A). Immunocytochemical analysis revealed colocalization of ectopically expressed Ptpcd1-myc with endogenous Plk1 (Fig. 2B). Intriguingly, Ptpcd1-myc appeared to accumulate and colocalize with Plk1 at mid-body in telophase cells. These results suggested that Ptpcd1 might also function in cytokinesis as Plk1 did [1]. To address this question, we examined the effect of Ptpcd1 overexpression on mitotic progression. Aberrant cytokinesis in the form of fused or intercellular α-tubulin bridges was apparent in cells expressing Ptpcd1 (Fig. 3A and C). Hence, an increase in the number of cells with multiple nuclei was observed when Ptpcd1 was overexpressed (Fig. 3B and C). These results suggested that Ptpcd1 as well as Plk1 as reported played an important role in cytokinesis.

In addition to cytokinesis, Plk1 was reported to stabilize microtubule organization [10,12]. Therefore, we then asked if Ptpcd1 expression affect the microtubule stabilization. HeLa cells were transfected with pcDNA3.1Ptpcd1-myc and treated with nocodaz-

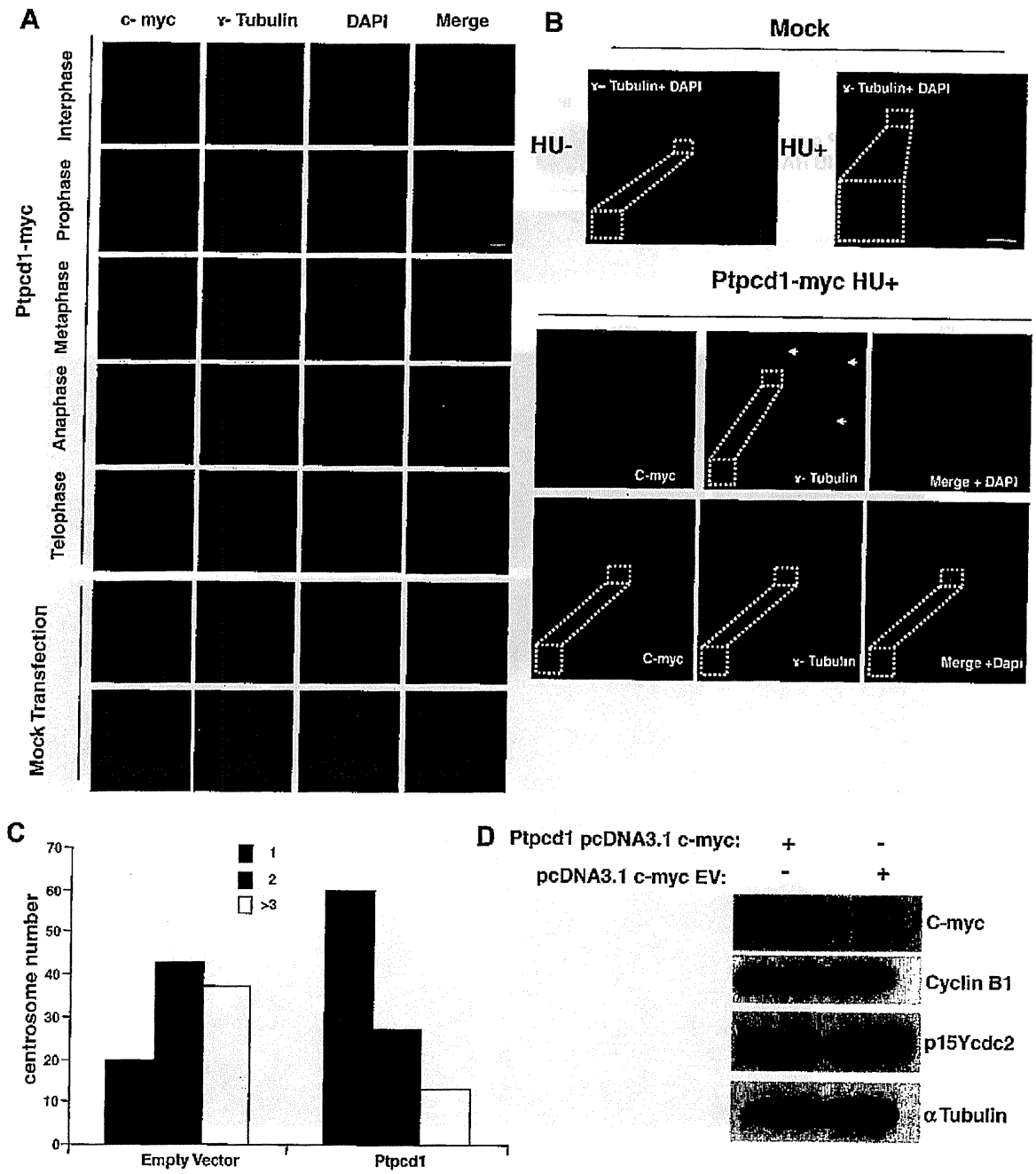

Fig. 1. Ptpcd1 localized to centrosomes and its overexpression prevents unscheduled centriole duplication. (A) Either Ptpcd1-myc or empty pcDNA3.1 as a negative control was transfected into HeLa cells. Cells were fixed with methanol and co-immunostained with γ-tubulin (green) and c-myc (red). DNA was counterstained with DAPI (blue). Scale bars; 5 μm. (B) Overexpression of Ptpcd1 prevents unscheduled centriole duplication. U2OS cells were transfected with either empty vector the presence or absence of HU (4 mM). (upper panels) or Ptpcd1-myc (lower panels) in the presence of HU (4 mM). Cells were then fixed and immunostained with anti-γ-tubulin antibodies (green) and c-myc (red). Arrows point at centrosomes, enlarged insets showed centrosomes. Scale bars; 5 μm. (C) The number of cells with 1, 2, or more than 2 centrosomes from (B) was counted and shown as a percentage of total cells. (D) Immunoblotting analysis. Whole cell extracts from (B) were subjected to immunoblotting using the indicate antibodies. (For interpretation of color mentioned in this figure the reader is referred to the web version of the article.)

ole, a microtubule depolymerizing agent. Overexpression of Ptpcd1-myc significantly stabilized microtubule organization when it was evaluated by staining with α-tubulin (Fig. 3D). Interestingly, it also enhanced microtubule regrowth after nocodazole washout. Thus, the effect of Ptpcd1-myc expression on microtubules stabilization was similar to that of Plk1 expression, further suggesting that Ptpcd1 functioned in Plk1-regulatory networks. In addition, these results also showed that the centrosomal localization of Ptpcd1 was independent of microtubules nucleation because centrosomal signals of Ptpcd1 could still be detected after microtubules depolymerization with nocodazole.

Overexpression of Ptpcd1 is capable of complementing prometaphase arrest in Plk1 depleted cells

We finally determined the genetic orientation between Plk1 and Ptpcd1. Endogenous Plk1 was depleted by the transfection of the specific siRNAs (D-1 and D-2) for Plk1. Immunoblotting using

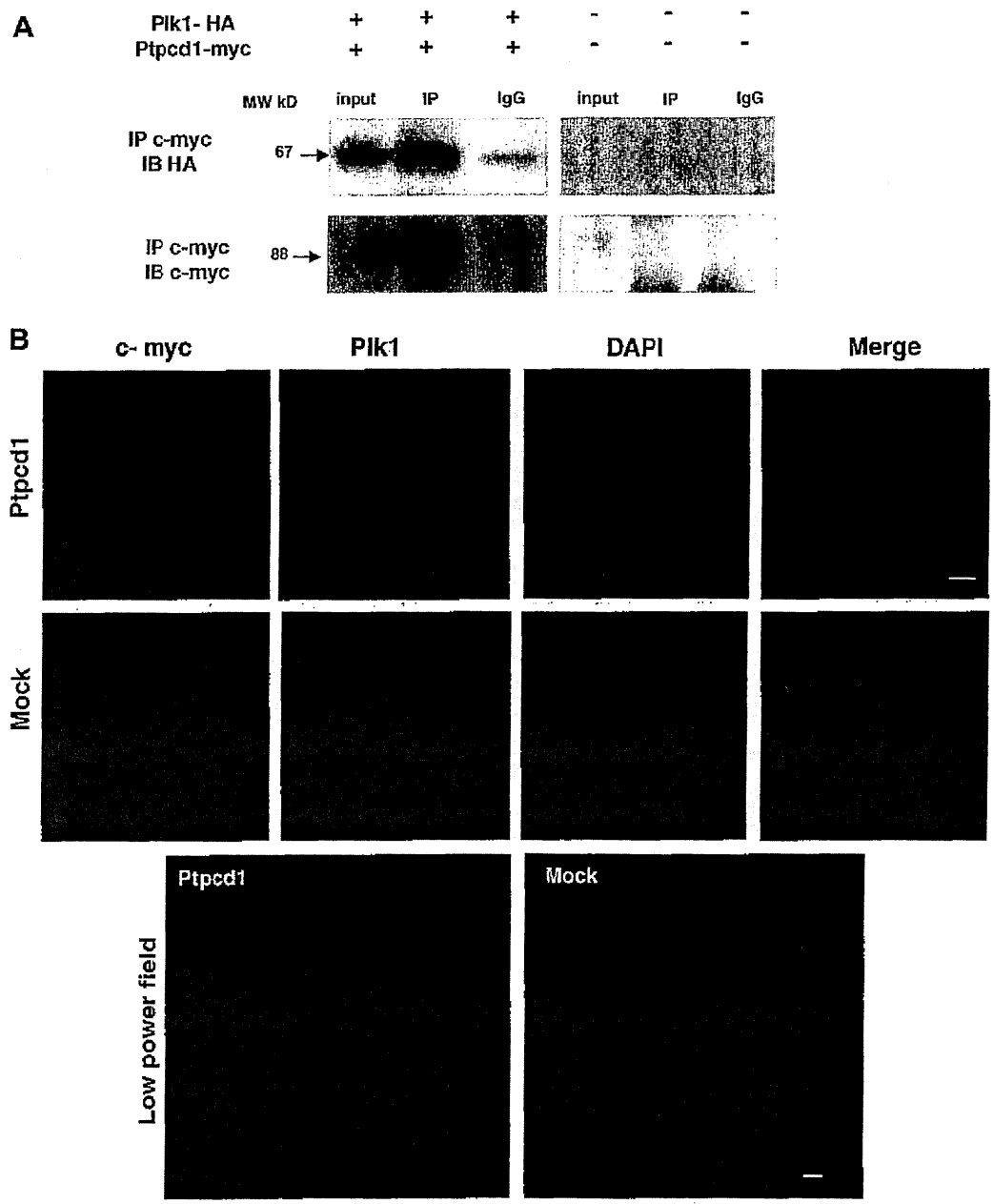

Fig. 2. Ptpcd1 interacted and colocalized with Plk1. U2OS cells were cotransfected with Plk1-HA and either Ptpcd1-myc or empty vectors (mock). Cells were harvested, and lysates were immunoprecipitated with anti-myc antibodies. Immunoprecipitates were subjected to immunoblotting using the indicated antibodies. (B) Colocalization of Ptpcd1 with Plk1. U2OS cells were transfected with Ptpcd1-myc and then stained with anti-myc antibodies (green) and anti-Plk1 antibodies (red, upper panels). DNA was counterstained with DAPI. Lower panels were low power fields of the upper images. Scale bars; 5 μm. (For interpretation of color mentioned in this figure the reader is referred to the web version of the article.)

anti-Plk1 antibodies revealed that transfection of D-1 and D-2 resulted in a significant reduction in Plk1 protein, whereas that of control siRNA did not (Fig. 4A). Plk1 depletion results in prometaphase/metaphase arrest [1], presumably due to impaired centrosomal separation, centrosome fragmentation, and microtubules destabilization, which consequently activate spindle checkpoints. Prolonged prometaphase arrest in Plk1 depleted cells ultimately appeared to induce apoptosis (Fig. 4B and Suppl. Fig. 2). Intriguingly, ectopic expression of Ptpcd1 in Plk1 depleted cells rescued the prometaphase/metaphase arrest and stabilized microtubules (Suppl. Fig. 2), but resulted in aberrant cytokinesis as was observed in Ptpcd1 expressing cells (Fig. 3C). These results indicated that Ptpcd1 at least in part functioned downstream of Plk1. Consistent with this notion, Ptpcd1 possessed four consensus serine residues for a Plk1 phosphorylation site (Fig. 4C) [26]. In this regard, Cdc5, a yeast homolog of Plks, regulated Cdc14p phosphorylation and its subcellular localization to ensure mitotic exit [14,27].

In summary, based on our observation in this study, it is possible that Ptpcd1 together with Plk1 may regulate the centriole duplication cycle as well as cytokinesis by modulating the phosphorylation status of some proteins, suggesting the conserved mechanism from yeast to mammalian by which Cdc5–Cdc14 axis regulates mitotic exit [1,14,27]. A similar counterbalance of kinase and phosphatase activities was also proposed in Nek2 and PP1α

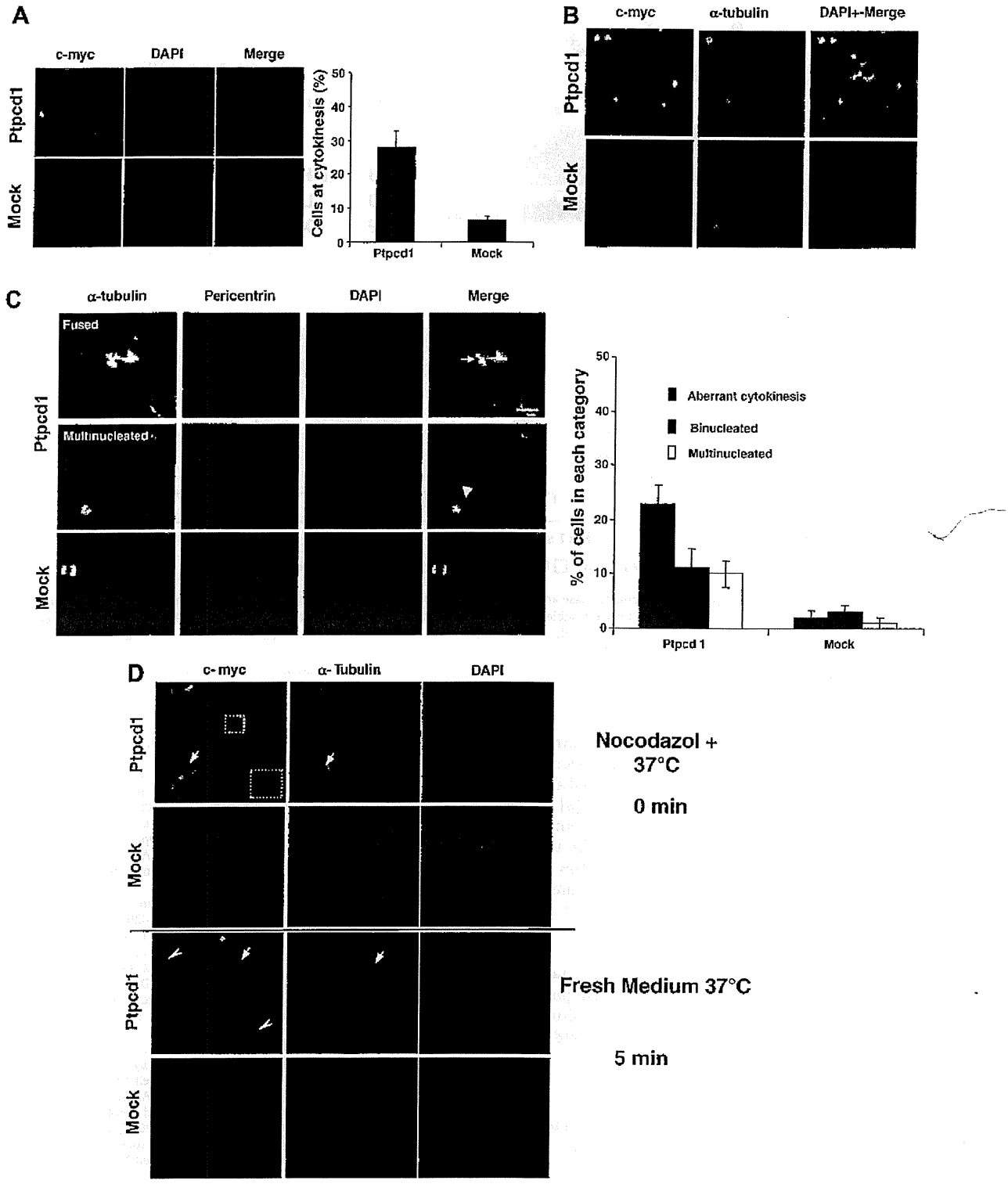

Fig. 3. Overexpression of Ptpcd1 resulted in aberrant cytokinesis and microtubules stabilization. (A) HeLa cells were transfected with either Ptpcd1-myc or empty vector (mock). Cells were immunostained with anti-myc (green) and DNA was counterstained with DAPI (blue). Scale bars; 5 μm (left panel). Cells with cytokinesis were counted and the data were presented as a percentage of total cells ($n > 200$) and means ± SD from three independent experiments (right panel). (B) HeLa cells were transfected as in (A) and stained with the indicated antibodies. DNA was counterstained with DAPI. (C) HeLa cells were transfected as in (B) and immunostained with anti-tubulin (red) and pericentrin (green). DNA was counterstained with DAPI. White arrow indicated persistent midbody structure and arrowhead pointed at multinucleated cells (left panels). Scale bars; 5 μm. Cells with aberrant cytokinesis, binucleated, and multinucleated cells from (left panels) were counted and the data were presented as a percentage of total cells ($n > 100$) and means ± SD from three independent experiments. (D) Microtubule regrowth assay. HeLa cells were transfected with either pcDNA3.1Ptpcd1-myc or empty vector. Cells were then treated with nocodazole as in Materials and Methods, and stained with anti-myc (green) and anti-α-tubulin (red) antibodies (upper panels). Cells were further cultured with the medium in the absence of nocodazole for 5 min and then stained as described above (lower panels). White arrow indicated stabilized α-tubulin bundles by Ptpcd1 and arrow head indicated newly growing microtubules. Insets show centrosomal Ptpcd1. Scale bars; 5 μm. (For interpretation of color mentioned in this figure the reader is referred to the web version of the article.)

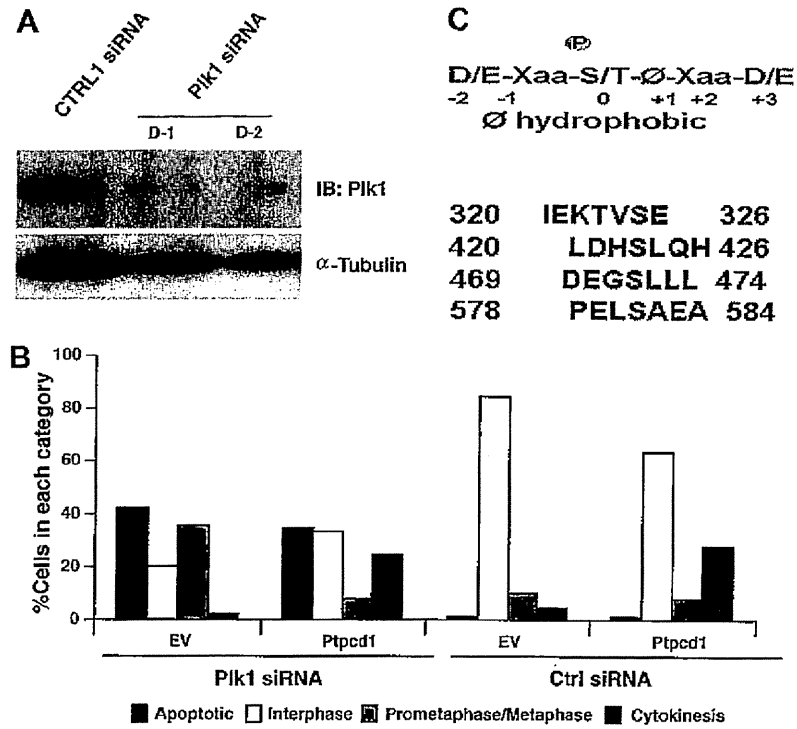

Fig. 4. Overexpression of Ptpcd1 rescued prometaphase/metaphase arrest observed in Plk1 depleted cells. (A) Plk1 depletion by transfection of its specific siRNAs. U2OS cells were transfected with the indicated siRNAs and the lysates were subjected to immunoblotting using the indicated antibodies. (B) U2OS cells were transfected with Ptpcd1 or empty vector (EV) as a negative control together with either Plk1 siRNA or control siRNA as indicated. The transfected cells were then fixed and immunostained stained with c-myc and α-tubulin. Cells in interphase, prometa/metaphase, cells with aberrant cytokinesis and/or underwent apoptosis were scored and the results were presented as a percentage of total cells ($n > 200$). (C) Schematic presentation of the predicted plk1 consensus phosphorylation site inside Ptpcd1 sequence. (For interpretation of color mentioned in this figure the reader is referred to the web version of the article.)

that governed centrosome splitting [4]. Although centrosomal and mitotic functions of mammalian Cdc14B had been described [15,17], Cdc14B deficient cells were viable and lacked apparent defects in chromosome segregation and cytokinesis [8], suggesting that alternative phosphatase(s) is being capable of complementing the mitotic functions of Cdc14B. Taken together with the fact that Ptpcd1 shared some sequence homology with Cdc14B, our results proposed that Ptpcd 1 might act as a functional isozyme to Cdc14B.

Acknowledgments

We thank Dr. Yamada-Namikawa for technical assistance and Dr. Majid Safwat for helpful discussion. This work was supported in part by the Ministry of Education, Science, Sports, and Culture of Japan through a Grant-in-Aid for Scientific Research (B) awarded to M.N.

Appendix A. Supplementary data

Supplementary data associated with this article can be found, in the online version, at doi:10.1016/j.bbrc.2009.01.113.

References

[1] T. Takaki, K. Trenz, V. Costanzo, M. Petronczki, Polo-like kinase 1 reaches beyond mitosis—cytokinesis, DNA damage response, and development, Curr. Opin. Cell Biol. 6 (2008) 650–660.
[2] L. Trinkle-Mulcahy, A.I. Lamond, Mitotic phosphatases: no longer silent partners, Curr. Opin. Cell Biol. 18 (2006) 623–631.
[3] K. Yuan, H. Hu, Z. Guo, G. Fu, A.P. Shaw, R. Hu, X. Yao, Phospho-regulation of HsCdc14A By polo-like kinase 1 is essential for mitotic progression, J. Biol. Chem. 282 (2007) 27414–27423.
[4] P. Meraldi, E.A. Nigg, Centrosome cohesion is regulated by a balance of kinase phosphatase activities, J. Cell Sci. 114 (2001) 3749–3757.
[5] C.G. Pearson, B.P. Culver, M. Winey, Centrioles want to move out and make cilia, Dev. Cell 13 (2007) 319–321.
[6] N. R Helps, X. Luo, H.M. Barker, P.T. Cohen, NIMA-related kinase 2 (Nek2), a cell cycle-regulated protein kinase localized to centrosomes, is complexed to protein phosphatase 1, Biochem. J. 349 (2000) 509–518.
[7] B.M. Lange, Integration of the centrosome in cell cycle control, stress response and signal transduction pathways, Curr. Opin. Cell Biol. 14 (2002) 35–43.
[8] P. Meraldi, J. Lukas, A.M. Fry, J. Bartek, E.A. Nigg, Centrosome duplication in mammalian somatic cells requires E2F and Cdk2-cyclin A, Nat. Cell Biol. 1 (1999) 88–93.
[9] F.A. Barr, H.H. Sillje, E.A. Nigg, Polo-like kinases and the orchestration of cell division, Nat. Rev. Mol. Cell Biol. 5 (2004) 429–440.
[10] I. Sumara, J.F. Gimenez-Abian, D. Gerlich, T. Hirota, C. Kraft, C. de la Torre, J. Ellenberg, J.M. Peters, Roles of polo-like kinase 1 in the assembly of functional mitotic spindles, Curr. Biol. 14 (2004) 1712–1722.
[11] P. Lenart, M. Petronczki, M. Steegmaier, B. Di Fiore, J.J. Lipp, M. Hoffmann, W.J. Rettig, N. Kraut, J.M. Peters, The small molecule inhibitor BI 2536 reveals novel insights into mitotic roles of polo-like kinase 1, Curr. Biol. 17 (2007) 304–315.
[12] M. Petronczki, M. Glotzer, N. Kraut, J.M. Peters, Polo-like kinase 1 triggers the initiation of cytokinesis in human cells by promoting recruitment of the RhoGEF Ect2 to the central spindle, Dev. Cell 12 (2007) 713–725.
[13] R. Neef, U. Gruneberg, R. Kopajtich, X. Li, E.A. Nigg, H. Sillje, F.A. Barr, Choice of Plk1 docking partners during mitosis and cytokinesis is controlled by the activation state of CdkI, Nat. Cell Biol. 9 (2007) 436–444.
[14] R. Visintin, F. Stegmeier, A. Amon, The role of the polo kinase Cdc5 in controlling Cdc14 localization, Mol. Biol. Cell 14 (2003) 4486–4498.
[15] J. Wu, H.P. Cho, D.B. Rhee, D.K. Johnson, J. Dunlap, Y. Liu, Y. Wang, Cdc14B depletion leads to centriole amplification, and its overexpression prevents unscheduled centriole duplication, J. Cell Biol. 181 (2008) 475–483.
[16] B.K. Kaiser, Z.A. Zimmerman, H. Charbonneau, P.K. Jackson, Disruption of centrosome structure, chromosome segregation, and cytokinesis by misexpression of human Cdc14A phosphatase, Mol. Biol. Cell 13 (2002) 2289–2300.
[17] H.P. Cho, Y. Liu, M. Gomez, J. Dunlap, M. Tyers, Y. Wang, The dual-specificity phosphatase CDC14B bundles and stabilizes microtubules, Mol. Cell Biol. 25 (2005) 4541–4551.
[18] E. Berdougo, M.V. Nachury, P.K. Jackson, P.V. Jallepalli, The nucleolar phosphatase Cdc14B is dispensable for chromosome segregation and mitotic exit in human cells, Cell Cycle 7 (2008) 1184–1190.

[19] T. Matsui, Y. Katsuno, T. Inoue, F. Fujita, T. Joh, H. Niida, H. Murakami, M. Itoh, M. Nakanishi, Negative regulation of Chk2 expression by p53 is dependent on the CCAAT-binding transcription factor NF-Y, J. Biol. Chem. 279 (2004) 25093–250100.
[20] M. Shimada, H. Niida, D.H. Zineldeen, H. Tagami, M. Tanaka, H. Saito, M. Nakanishi, Chk1 is a histone H3 threonine 11 kinase that regulates DNA damage-induced transcriptional repression, Cell 132 (2008) 221–232.
[21] H. Niida, Y. Katsuno, B. Banerjee, M.P. Hande, M. Nakanishi, Specific role of Chk1 phosphorylations in cell survival and checkpoint activation, Mol. Cell Biol. 27 (2007) 2572–2581.
[22] O.V. Plotnikova, E.A. Golemis, E.N. Pugacheva, Cell cycle-dependent ciliogenesis and cancer, Cancer Res. 68 (2008) 2058–2061.
[23] A. Spektor, W.Y. Tsang, D. Khoo, B.D. Dynlacht, Cep97 and CP110 suppress a cilia assembly program, Cell 130 (2007) 678–690.
[24] L.M. Quarmby, M.R. Mahjoub, Caught Nek-ing: cilia and centrioles, J. Cell Sci. 118 (2005) 5161–5169.
[25] T.S. McClintock, C.E. Glasser, S.C. Bose, D.A. Bergman, Tissue expression patterns identify mouse cilia genes, Physiol. Genomics 32 (2008) 198–206.
[26] H. Nakajima, F. Toyoshima-Morimoto, E. Taniguchi, E. Nishida, Identification of a consensus motif for Plk (Polo-like kinase) phosphorylation reveals Myt1 as a Plk1 substrate, J. Biol. Chem. 278 (2003) 25277–25280.
[27] C. Visintin, B.N. Tomson, R. Rahal, J. Paulson, M. Cohen, J. Taunton, A. Amon, R. Visintin, APC/C-Cdh1-mediated degradation of the Polo kinase Cdc5 promotes the return of Cdc14 into the nucleolus, Genes Dev. 22 (2008) 79–90.

EXPERIMENTAL CELL RESEARCH 315 (2009) 809–819

available at www.sciencedirect.com

ScienceDirect

www.elsevier.com/locate/yexcr

Research Article

Disruption of the novel gene *fad104* causes rapid postnatal death and attenuation of cell proliferation, adhesion, spreading and migration

Makoto Nishizuka[a], *Keishi Kishimoto*[a], *Ayumi Kato*[a], *Masahito Ikawa*[b], *Masaru Okabe*[b], *Ryuichiro Sato*[c], *Hiroyuki Niida*[d], *Makoto Nakanishi*[d], *Shigehiro Osada*[a], *Masayoshi Imagawa*[a,*]

[a]*Department of Molecular Biology, Graduate School of Pharmaceutical Sciences, Nagoya City University, 3-1 Tanabe-dori, Mizuho-ku, Nagoya, Aichi 467-8603, Japan*

[b]*Genome Information Research Center, Osaka University, Yamadaoka 3-1, Suita, Osaka 565-0871, Japan*

[c]*Department of Applied Biological Chemistry, Graduate School of Agricultural and Life Sciences, The University of Tokyo, Tokyo 113-8657, Japan*

[d]*Department Cell Biology and Biochemistry, Graduate School of Medical Sciences, Nagoya City University, 1 Kawasumi, Mizuho-cho, Mizuho-ku, Nagoya, Aichi 467-8601, Japan*

ARTICLE INFORMATION

Article Chronology:
Received 17 July 2008
Revised version received
9 November 2008
Accepted 12 December 2008
Available online 29 December 2008

Keywords:
fad104
Adipocyte differentiation
Cell proliferation
Cell adhesion
Cell spreading
Cell migration

ABSTRACT

The molecular mechanisms at the beginning of adipogenesis remain unknown. Previously, we identified a novel gene, *fad104* (factor for adipocyte differentiation 104), transiently expressed at the early stage of adipocyte differentiation. Since the knockdown of the expression of *fad104* dramatically repressed adipogenesis, it is clear that *fad104* plays important roles in adipocyte differentiation. However, the physiological roles of *fad104* are still unknown. In this study, we generated *fad104*-deficient mice by gene targeting. Although the mice were born in the expected Mendelian ratios, all died within 1 day of birth, suggesting *fad104* to be crucial for survival after birth. Furthermore, analyses of mouse embryonic fibroblasts (MEFs) prepared from *fad104*-deficient mice provided new insights into the functions of *fad104*. Disruption of *fad104* inhibited adipocyte differentiation and cell proliferation. In addition, cell adhesion and wound healing assays using *fad104*-deficient MEFs revealed that loss of *fad104* expression caused a reduction in stress fiber formation, and notably delayed cell adhesion, spreading and migration. These results indicate that *fad104* is essential for the survival of newborns just after birth and important for cell proliferation, adhesion, spreading and migration.

© 2008 Elsevier Inc. All rights reserved.

* *Corresponding author.* Fax: +81 52 836 3455.
E-mail address: imagawa@phar.nagoya-cu.ac.jp (M. Imagawa).

Abbreviations: fad104, factor for adipocyte differentiation 104; BAT, brown adipose tissue; C/EBP, CCAAT/enhancer binding protein; Dex, dexamethasone; ER, endoplasmic reticulum; FBS, fetal bovine serum; FITC, fluorescein isothiocyanate; FNDC3a, fibronectin type III domain containing 3a; GFP, green fluorescent protein; H&E, hematoxylin and eosin; IBMX, 3-isobutyl-1-methylxantine; Ins, insulin; LC3, microtubule-associated protein light chain; MEFs, mouse embryonic fibroblasts; PBS, phosphate-buffered saline; PCR, polymerase chain reaction; PPARγ, peroxisome proliferator-activated receptor γ; RACE, rapid amplification of cDNA ends; RGS2, regulators of G protein signaling 2; SREBP-1, sterol regulatory element-binding protein 1; sys, symplastic spermatids; TCL/TC10βL, TC10 like/TC10βLong; TRITC, tetramethylrhodamine isothiocyanate; TUNEL, TdT-mediated dUTP-biotin nick end labeling; WAT, white adipose tissue

0014-4827/$ – see front matter © 2008 Elsevier Inc. All rights reserved.
doi:10.1016/j.yexcr.2008.12.013

Author's personal copy

Introduction

Obesity is a risk factor for many diseases, such as diabetes, hypertension, hyperlipoidemia, and also arteriosclerosis [1]. Obesity is the result of an expansion of individual adipocytes and increase in the overall number of adipocytes. Therefore, to clarify the mechanism of obesity, it is necessary to elucidate the molecular mechanisms by which adipocytes differentiate. It is well established that peroxisome proliferator-activated receptor γ (PPAR γ), the CCAAT/enhancer-binding protein (C/EBP) family, and sterol regulatory element-binding protein 1 (SREBP-1) have crucial roles in the middle and the late stages of the differentiation process [2,3]. However, the events early on in adipogenesis are not fully understood.

Previously, we isolated 102 genes as inducible during the earliest stage of adipocyte differentiation with a polymerase chain reaction (PCR)-subtraction protocol [4,5]. We have identified regulators of G protein signaling 2 (RGS2), TC10-like/TC10βLong (TCL/TC10βL) and p68 RNA helicase as factors accelerating the differentiation process [6–8]. In addition, it was of interest that almost half of the isolated genes were unknown, not being present in the databases. Using the rapid amplification of cDNA ends (RACE) technique and cDNA library screening, we identified four novel genes, factor for adipocyte differentiation 24 (*fad24*), *fad123*, *fad158* and *fad104* [9–12]. Furthermore, we reported that *fad24*, *fad158* and *fad104* were positive regulators of adipocyte differentiation [9,11–13].

FAD104 is a novel protein containing 9 repeats of the fibronectin type III domain and a transmembrane domain. The expression of *fad104* was quickly and transiently elevated at the early stage of adipogenesis and was restricted to the differentiable state. Moreover, the knockdown of *fad104* by RNA interference caused inhibition of the differentiation of 3T3-L1 preadipocytes [12]. These results indicated *fad104* to have an important role in the differentiation.

The fibronectin type III domain contained in FAD104 is found in cell surface receptors and proteins regulating cell adhesion such as fibronectin and vitronectin [14,15]. Fibronectin is one of the extracellular matrix proteins and consists of three types of repeating module, called type I, type II and type III repeats. Fibronectin binds to a variety of extracellular and cell surface molecules, including integrins α5β1 and α4β1 and the HSPG coreceptor syndecan 4, and regulates cell adhesion, spreading, migration, growth and differentiation [16,17]. The Arg-Gly-Asp (RGD) tripeptide sequence in the type III_{10} module of fibronectin plays an important role in the binding of the integrin receptor and activating of integrin-mediated intracellular signals [18,19]. It is of interest that *fad104* also has a RGD tripeptide sequence in the eighth fibronectin type III domain.

In addition, some previous reports indicate that the extracellular matrix proteins including fibronectin and integrins have important roles in adipogenesis [20,21]. The expression of fibronectin and integrin is downregulated during adipogenesis [20]. Furthermore, it was reported that the disruption of contacts with the extracellular matrix was required for adipocyte differentiation [21]. These reports indicate the importance of interaction between the differentiating cells and extracellular matrix, suggesting that the proteins containing the fibronectin type III domain have some crucial role in the differentiation process. However, the role of *fad104* in adipocyte conversion and various cellular functions including cell proliferation, adhesion, spreading and migration is unclear.

In this study, to gain insight into the physiological role of *fad104 in vivo*, we generated mice lacking *fad104*. Although born in the expected Mendelian ratios, the *fad104*-deficient mice all died within 1 day after birth. Interestingly although FAD104 possesses 9 repeats of the fibronectin type III domain, FAD104 localized to the endoplasmic reticulum (ER). Furthermore, analyses of mouse embryonic fibroblasts (MEFs) prepared from *fad104*-deficient mice revealed that disruption of *fad104* caused a reduction in the ability to differentiate, proliferate, adhere, spread and migrate. These results indicate that the novel gene *fad104* is essential for the survival of neonates and promotes not only adipocyte differentiation, but also cell proliferation, adhesion, spreading and migration.

Materials and methods

Generation of the fad104 knockout mouse

The targeting vector was constructed by ligating a 1.0 kb *Xho* I fragment and a 4.4 kb *Xho* I-*Sal* I fragment, which were located upstream and downstream of exon 2, respectively, to the pgk-neo cassette of pLNTK. Both the *Xho* I and *Xho* I-*Sal* I fragments were amplified by PCR using genomic DNA prepared at E14 as a template. The pgk-tk expression cassette was placed next to the short arm for negative selection against random integration. The targeting construct was linearized with the *Sal* I site and electroporated into D3 ES cells. Three positive ES cell clones, screened by Southern blot analyses, were microinjected into C57BL/6 Cr blastocysts purchased from Japan SLC (Shizuoka, Japan). The blastocysts were transferred to ICR pseudopregnant females, resulting in the birth of three lines of male chimeric mice. These male chimeric offspring were mated with C57BL/6 females and chimeras from two lines exhibited germ-line transmission. The F1 agouti offspring mice were then analyzed by Southern blotting and PCR analyses. Heterozygote male mice were backcrossed onto the C57BL/6 background for more than seven generations. All experiments were carried out according to the Guideline for the Care and Use of Laboratory Animals of Nagoya City University Medical School.

Genotyping

For Southern blot analyses, genomic DNA from ES cells and tail snippets was digested with *Bam*HI-*Bgl*II, fractionated on a 1% agarose gel, and blotted onto a Hybond N+ nylon membrane (Amersham Biosciences). Homologous recombination was determined by using as a probe, 500 bp fragments located outside the targeting vector. The filter was hybridized with a probe labeled with [α-^{32}P]-dCTP using a random labeling kit (Takara Biomedicals). The wild-type allele produces a DNA sequence of 5. 4 kb, while the targeted DNA is 2. 0 kb long (Fig. 1A).

Measurements of body temperature, blood glucose level and brown adipose tissue (BAT) weight

Newborn pups were obtained by caesarean delivery at E18.5. Just after caesarean section, a thermistor (PHYSITEMP INSTRUMENTS INC.) was introduced into the rectum of pups for body temperature measurements. BAT was isolated from the interscapular space of newborn pups, and measured its weight. Blood

Author's personal copy

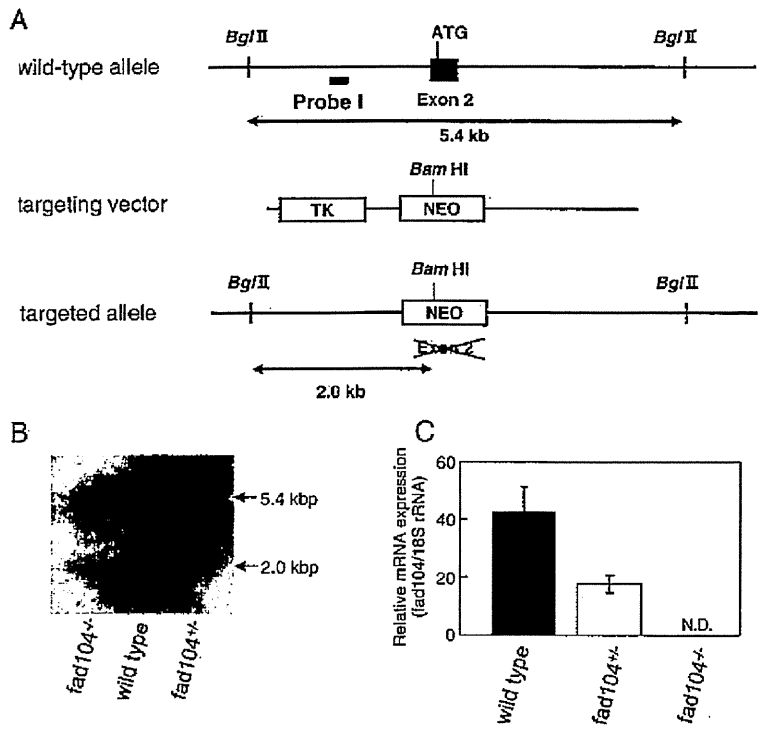

Fig. 1 – Targeted disruption of the *fad104* gene. (A) Schematic representation of the wild-type and targeted alleles. The black box represents exon 2 of the *fad104* gene. The white boxes represent pgk-neo and pgk-tk cassettes. The probe used for Southern blot analysis is shown as Probe I. (B) Southern blot analysis of mouse genomic DNA. The expected DNA fragments for the targeted allele and the wild-type allele are 2.0 and 5.4 kb, respectively. (C) Q-PCR analysis of mRNA from embryonic fibroblasts isolated from each of the genotypes. The expression level of *fad104* was normalized with 18S rRNA expression determined by Q-PCR. The data represent means with standard deviations (n=3).

glucose level was measured by the Glucose CII-Test (Wako Pure Chemical).

Preparation of MEFs and adipocyte differentiation

MEFs were isolated from decapitated embryonic day 13.5 embryos of wild type and *fad104*$^{-/-}$ mice. According to the previous reports, MEFs were used at low passage numbers (2 to 4 times) throughout the studies to avoid accumulative genetic abnormalities during passage [22,23]. Cells were cultured in α-modified Eagle's medium (α-MEM; Invitrogen) supplemented with 10% fetal bovine serum (FBS).

Induction of adipogenic differentiation was carried out according to methods described previously [24]. Briefly, MEFs (2 times passage) were seeded in culture dishes. The medium was changed to α-MEM supplemented with 0.5 mM 3-isobutyl-1-methylxantine (IBMX), 5 μg/ml of insulin (Ins), 1 μM dexamethasone (Dex), and 10% FBS at 2 days postconfluence. This medium was renewed every other day. The amounts of triacylglycerol were measured using LIPIDOS LIQUID (Ono) according to the manufacturer's instructions.

Implantation and histological analyses

MEFs (4 times passage) were grown to near confluence and trypsinized. After centrifugation, cell pellets were suspended in α-MEM containing 10% FBS and injected subcutaneously (3×10^7 cells per site) with a 21-gauge needle at the back of BALB/c athymic mice (Charles River Laboratories). Three weeks after implantation, these mice were killed by cervical dislocation, and the fat pads derived from the implanted cells were excited and fixed in 10% formalin in phosphate-buffered saline (PBS). The specimens were cut into 4-μm-thick sections and stained with hematoxylin and eosin (H&E). For lipid staining with osmium tetroxide (OsO_4), the retrieved implants were fixed in 2.5% glutaraldehyde in PBS for 15 min and 10% formalin in PBS. To cross-link intracellular lipids, the implants were covered with a 1% OsO_4 solution for 2 h on ice. After excess OsO_4 was removed by washing with distilled water, the implants were fixed again with 10% formalin in PBS, and embedded in paraffin. The specimens were cut into 6-μm-thick sections and deparaffinized to observe OsO_4-stained lipids.

Real-time quantitative RT-PCR (Q-PCR)

Total RNA was extracted using TRIzol (Invitrogen). For Q-PCR, cDNA was prepared using ReverTra Ace-α- (TOYOBO) following the manufacturer's recommended procedures. An ABI PRISM 7000 sequence detection system (Applied Biosystems) was used to perform Q-PCR. The pre-designed primers and probe sets of *fad104* and 18S rRNA were obtained from Applied Biosystems. The reaction mixture was prepared using a TaqMan Universal PCR

Author's personal copy

Master Mix (Applied Biosystems) according to the manufacturer's instructions. The mixture was incubated at 50 °C for 2 min and at 95 °C for 10 min, and then the PCR was done at 95 °C for 15 s and at 60 °C for 1 min for 40 cycles. The relative standard curves were generated in each experiment to calculate the input amounts of the unknown samples.

Subcellular localization of FAD104

An amino terminal Flag tagged FAD104 expression plasmid, pFlag-fad104, and a carboxy terminal green-fluorescent protein (GFP) tagged FAD104 expression plasmid, pfad104-GFP, were constructed by subcloning the coding region of *fad104* into p3xFlag-CMV7.1 (SIGMA) and pEGFP-N1 (BD Biosciences), respectively.

NIH-3T3 cells were plated onto cell disks (SUMITOMO BAKELITE Co., Ltd) 1 day before transfection. The cells were transfected using the calcium co-precipitation method, fixed with 2% paraformaldehyde in PBS and permeabilized with 0.2% Triton X-100. Each cell disk was incubated with primary antibody, rabbit polyclonal anti-calnexin antibody (H-70) (Santa Cruz Biotechnology) and mouse monoclonal anti-Flag antibody (SIGMA), for 1 h at room temperature. After 5 washes with PBS, tetramethylrhodamine isothiocyanate (TRITC)-conjugated anti-rabbit and fluorescein isothiocyanate (FITC)-conjugated anti-mouse antibodies were reached for 1 h at room temperature. After 5 washes with PBS, the signals for GFP, FITC and TRITC were detected by confocal laser scanning microscopy (LSM510META, Carl Zeiss Co., Ltd).

Cell proliferation and cell death assay

Two times passage MEFs were used in this study. The cells (3×10^4) were seeded into 6-well tissue culture plates and trypsinized. Numbers of cells were counted at various time points during the cell growth period. For the detection of cell death, TdT-mediated dUTP-biotin nick end labeling (TUNEL) assays were performed using the In Situ Cell Death Detection kit, Fluorescein (Roche) according to the manufacturer's instructions.

Cell adhesion assay

Four times passage MEFs were used in this study. The cells (1×10^4) were plated onto fibronectin-coated (3 μg/ml) 24-well plates. For the coating of fibronectin, human fibronectin (SIGMA) was incubated for 1 h at room temperature. At specific time points, the unattached cells were washed away with PBS. The attached cells were fixed for 10 min in 2% paraformaldehyde in PBS at room temperature. After 3 washes with PBS, the attached cells were photographed, and counted in five random microscopic fields per plate.

Immunofluorescence microscopy

Four times passage MEFs were used in this study. MEFs (4×10^4) were replated on fibronectin-coated (3 μg/ml) cell disks in 24-well plates. At different time points, cell disks were fixed for 10 min in 2% paraformaldehyde in PBS and permeabilized with 0.2% Triton X-100. The cell disks were incubated with anti-vinculin monoclonal antibody (SIGMA) for 1 h at room temperature. After 3 washes with PBS, FITC-conjugated anti-mouse secondary antibody and TRITC-conjugated phalloidin (Jackson ImmunoResearch) for detection of the F-actin structure of the cells were reacted for 1 h at room temperature. After 3 more washes with PBS, FITC and TRITC signals were detected by fluorescence microscopy (BX51, OLYMPUS).

Wound healing assay

Four times passage MEFs were used in this study. MEFs of wild-type and *fad104*$^{-/-}$ mice were grown to confluence in 60 mm dishes. At 1 day postconfluence, four sites in each plate were scraped with a yellow plastic pipette tip to generate scratch wounds. The medium was removed and replaced with fresh medium. The cells were incubated at 37 °C for 10 h. The wound areas at various points were photographed and measured using NIH-Image J software.

Statistical analyses

Data are expressed as the mean±standard deviation (S.D.) or the mean±standard error (S.E.). All data presented with statistical analyses were analyzed using a Student's *t* test. *p* values less than 0.05 were considered to be significant.

Results

Disruption of the fad104 gene causes rapid postnatal death

To explore the function of *fad104 in vivo*, we generated *fad104*-deficient mice. We previously indicated that the mouse *fad104* was located at chromosome 3 and constituted 26 exons [12]. To disrupt the *fad104* gene, the targeting vector was designed to remove the second exon of *fad104*, which included the translational start site (Fig. 1A). The targeting vector was introduced into D3 ES cells and positive cells were selected using G418 and ganciclovir. Three of the targeted ES cell lines were injected into C57BL/6 Cr blastocysts, and chimeric male mice were obtained. Of these, two lines of mice exhibited germ-line transmission. Intercrosses of the heterozygote mice were used to establish the homozygote *fad104*-deficient mice.

First, we analyzed the genotype of mice in the heterozygote intercross at 4 weeks of age. However, *fad104*$^{-/-}$ mice were not found among 55 live-born progenies. Then, we observed the fate of the newborn mice at 1 day of birth. As shown in Table 1, ten of 47 pups obtained from crosses between heterozygote mice had already died, and three more pups died the next day. Southern blot analysis indicated that 13 newborns that died within 1 day of birth were homozygous mutants, which is almost equal to the expected Mendelian ratio (Table 1, Fig. 1B). Furthermore, Q-PCR analysis using MEFs prepared from offspring of the heterozygote intercross confirmed that *fad104*-deficient mice do not express *fad104* (Fig. 1C).

Table 1 – Genotype of progeny of heterozygote intercrosses

Age	No. of mice with genotype		
	+/+	+/−	−/−
E 18.5	9	24	13
P1	13	21	13[a]
4-week	19	36	0

[a] Ten newborns had died. Another 3 newborns died within 1 day.

Author's personal copy

To determine whether disruption of *fad104* causes lethality during embryogenesis, we next examined the genotype of newborns from the heterozygote intercross at E18.5. Just minutes after caesarean section, all pups at E18.5 were alive, and exhibited the expected Mendelian ratio (Table 1). However, all the *fad104*$^{-/-}$ offspring died within 15 min after caesarean section, whereas the wild-type and *fad104*$^{+/-}$ neonates survived. Similar results were observed for other *fad104*-deficient mice, which were obtained from independent ES clones. These results strongly suggest that the disruption of *fad104* causes rapid postnatal death.

To clarify the causes of rapid postnatal death by the disruption of *fad104*, we examined whether *fad104* is involved in the energy homeostasis just after birth (Fig. 2). We first measured the body weights and blood glucose levels of *fad104*$^{-/-}$ neonates. The body weights and blood glucose levels of *fad104*$^{-/-}$ neonates were not significantly different from those of wild-type and *fad104*$^{+/-}$ pups (Figs. 2A and B). Just after birth, the thermoregulation is very important to maintain energy homeostasis. Therefore, we next measured the body temperatures of newborn pups just after caesarean. The body temperatures did not differ among three genotypes (Fig. 2C). Furthermore, we measured weights of BAT isolated from the interscapular space of neonates. The weights of BAT of *fad104*$^{-/-}$ neonates were not also different from those of wild-type and *fad104*$^{+/-}$pups (Fig. 2D). These results may indicate that the rapid postnatal death observed in *fad104*-deficient infants is not caused by the failure of energy homeostasis.

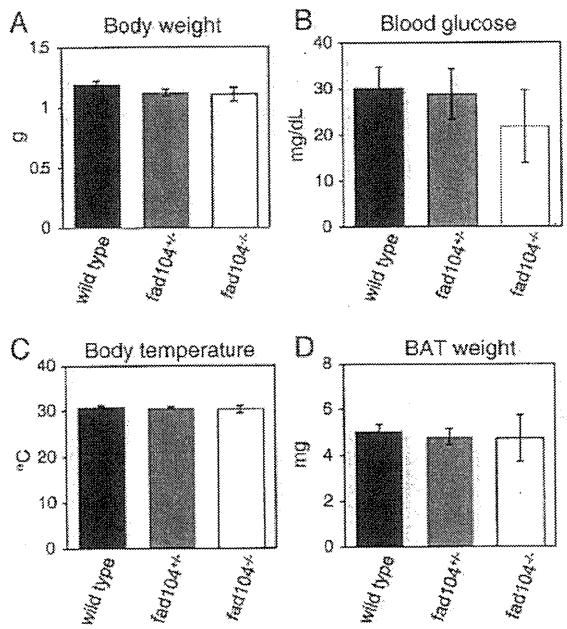

Fig. 2 – Characterization of *fad104*-deficient mice at embryonic day 18.5. Body weights, blood glucose levels, body temperatures and BAT weights of neonates were measured just after caesarean section. (A) Body weights (wild-type, $n=17$, *fad104*$^{+/-}$, $n=36$, *fad104*$^{-/-}$, $n=9$). (B) Body temperatures (wild-type, $n=10$, *fad104*$^{+/-}$, $n=11$, *fad104*$^{-/-}$, $n=4$). (C) Blood glucose levels (wild-type, $n=12$, *fad104*$^{+/-}$, $n=14$, *fad104*$^{-/-}$, $n=5$). (D) BAT weights (wild-type, $n=10$, *fad104*$^{+/-}$, $n=11$, *fad104*$^{-/-}$, $n=4$). Each column represents the mean with standard error.

Fad104-deficient MEFs exhibit reduced adipogenesis

Since the disruption of *fad104* causes postnatal death, it is clear that *fad104* has an important role in the survival of newborn. Our previous report indicated that *fad104* promoted the differentiation of 3T3-L1 preadipocytes [12]. Therefore, using the MEFs prepared from *fad104*-deficient mice, we first examined the role of *fad104* in the conversion to adipocytes.

We investigated the expression of *fad104* during the differentiation of MEFs prepared from wild-type embryos. The level of *fad104* quickly elevated after the induction, and reached a peak at 3 h as found in 3T3-L1 cells (Fig. 3A). Next, we performed a differentiation experiment. Wild-type and *fad104*$^{-/-}$ MEFs were brought to confluence in 10% FBS. After 2 days of incubation, the medium was changed to the differentiated medium. After 12 days, the cells were stained with Oil Red O to detect oil droplets (Fig. 3B) and the amounts of triacylglycerol were determined (Fig. 3C). Under these conditions, approximately 50% of MEFs from wild-type embryos could differentiate into adipocytes. On the other hand, little accumulation of oil droplets and triacylglycerol in MEFs from *fad104*$^{-/-}$ embryos was observed.

Next, MEFs prepared from wild-type and *fad104*$^{-/-}$ embryos were implanted subcutaneously into the back of athymic mice. After 3 weeks, the implants were excited. The weights of the implants derived from *fad104*$^{-/-}$ MEFs were indistinguishable from those of wild-type MEFs (data not shown). In order to observe the histological characterization of implants, the cells accumulated oil droplets were detected by H&E and OsO_4 staining. The implanted wild-type MEFs developed into adipocytes and stored oil droplets. In contrast, the implanted *fad104*$^{-/-}$ MEFs failed to develop into mature adipocytes (Fig. 4). These results combined with our previous observations demonstrated that *fad104* has an important role for the differentiation of MEFs as well as of mouse 3T3-L1 cells.

FAD104 localized to the endoplasmic reticulum (ER)

To determine the subcellular localization of FAD104, Flag-fad104 chimeric plasmid was transiently introduced into NIH-3T3 cells and the signals were detected by confocal scanning laser microscopy. The signals of Flag-FAD104 were observed in the cytoplasm (Fig. 5A). Because FAD104 possesses a transmembrane domain at the C-terminus, it seems that FAD104 distributes to the membrane structure in the cytoplasm. Therefore, we further conducted immunofluorescent staining using antibody against calnexin, which is a marker for the ER. The distribution of Flag-FAD104 overlapped with the staining pattern of calnexin (Fig. 5A). Since Flag-fad104 chimeric construct have Flag tag at the N-terminal site, we further constructed fad104-GFP chimeric plasmid in which GFP stays in the C terminus and introduced into NIH-3T3 cells. As shown in Fig. 5B, FAD-GFP was also distributed in the cytosol and overlapped with calnexin. These results demonstrated that the type and position of tags do not affect the distribution and FAD104 localized to the ER.

Cell proliferation was inhibited in fad104-deficient MEFs

The experiments of subcellular localization of FAD104 demonstrated that FAD104 is a novel ER protein. However, it is unclear whether *fad104* is involved in cellular functions including cell proliferation, cell adhesion, cell spreading and cell migration. To elucidate the function of *fad104*, we further analyzed *fad104*-deficient MEFs.

Author's personal copy

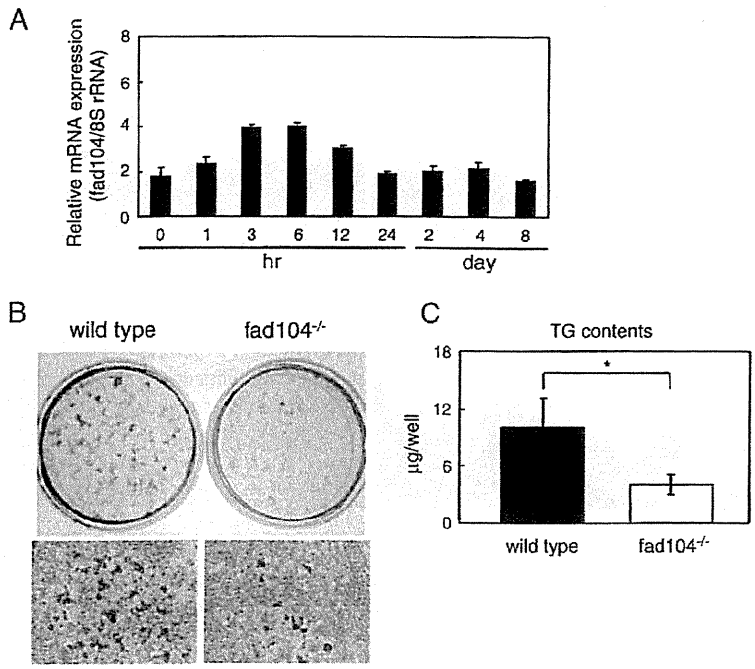

Fig. 3 – Adipocyte differentiation of MEFs from wild-type and homozygous *fad104*-deficient embryos. (A) Q-PCR analyses of *fad104* expression in MEFs from wild-type embryos. The expression level of *fad104* was determined at various time points in the differentiation of MEFs from wild-type embryos and normalized with 18S rRNA expression determined by Q-PCR. The data represent means with standard deviations ($n=3$). (B) Differentiation of MEFs from wild-type and *fad104*$^{-/-}$ embryos. Wild-type and *fad104*$^{-/-}$ MEFs were treated with the differentiation medium containing IBMX, Dex, Ins and FBS. These cells after 12 days treatment were stained with Oil Red O. Oil Red O staining of plates (upper) and microscopic examination (lower). (C) The amounts of triacylglycerol. The measurement of triacylglycerol content was done on 24-well plates. Each column represents the mean with standard deviations ($n=3$). *$p<0.05$.

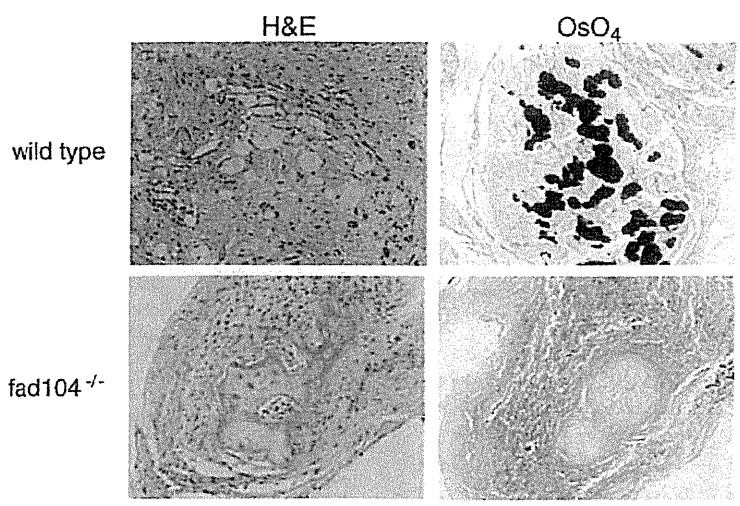

Fig. 4 – Histological analyses of the implanted MEFs from wild-type and fad104-deficient embryo. At 3 weeks after implantation of MEFs prepared from wild-type (upper panels) and *fad104*$^{-/-}$ (lower panels) embryos, the implants were excited and stained by H&E (left panels) and OsO_4 (right panels).

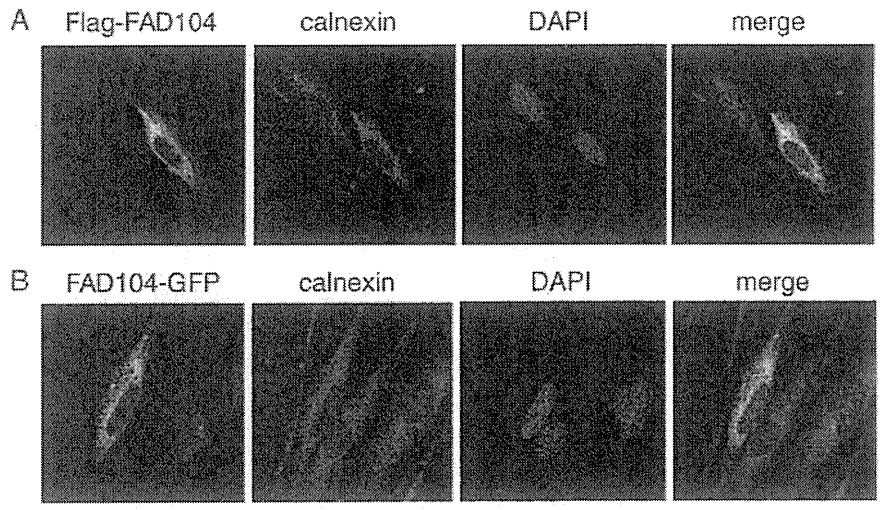

Fig. 5 – Subcellular localization of FAD104. (A) Subcellular localization of Flag-FAD104. NIH-3T3 cells were transiently transfected with Flag-*fad104*-expression plasmid. After conducting immunofluorescent staining using anti-Flag and anti-calnexin, the signals of Flag-FAD104 (green) and calnexin (red) were detected with confocal laser scanning microscopy. (B) Subcellular localization of FAD104-GFP. NIH-3T3 cells were transiently transfected with *fad104*-GFP-expression plasmid. Transfected NIH-3T3 cells were fixed and performed the immunofluorescence analyses staining with anti calnexin. Fluorescence of FAD104-GFP (green) and calnexin (red) were detected with confocal laser scanning microscopy.

First, we investigated the rate of cell proliferation of wild-type and *fad104*$^{-/-}$ MEFs. MEFs prepared from wild-type and *fad104*$^{-/-}$ embryos were seeded in tissue cultures, and counted at various time points. As shown in Fig. 6, the *fad104*-deficient MEFs exhibited a slightly decrease in proliferation compared with the wild-type MEFs. To exclude the possibility that the decrease of proliferating rate by the disruption of *fad104* was caused by the increase the cell death including anoixis, we performed TUNEL assay to detect cell death during proliferation in MEFs prepared from wild-type and *fad104*$^{-/-}$ embryos. At 2, 4, and 6 days after seeding, no TUNEL-positive cells were observed in wild-type and *fad104*$^{-/-}$ MEFs (data not shown). The difference of cell proliferation between wild-type and *fad104*$^{-/-}$ MEFs may not be caused by cell death. These results indicated that the disruption of *fad104* inhibits cell proliferation.

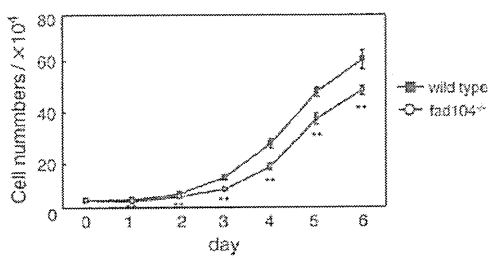

Fig. 6 – Cell proliferation was inhibited in *fad104*-deficient MEFs. MEFs from wild-type and *fad104*$^{-/-}$ embryos were seeded in 6-well tissue culture plates at a total 3×10^4 cells/well. These cells were trypsinized and counted. The data represent means with standard deviations ($n=4$) $^{**}p<0.01$.

Deficiency of fad104 reduced stress fiber formation and caused a delay in cell adhesion and cell spreading

Next, to examine the effect of disruption of *fad104* on cell adhesion, cell spreading and the actin cytoskeleton's organization, we stained F-actin of wild-type and *fad104*$^{-/-}$ MEFs with TRITC-conjugated phalloidin. In addition, to detect the focal complex in wild-type and *fad104*$^{-/-}$ MEFs, the localization of vinculin was visualized using anti-vinculin antibody.

At 30 min from seeding, the wild-type MEFs already showed cell spreading and the formation of long actin stress fibers. In contrast, the *fad104*$^{-/-}$ MEFs were significantly delayed in spreading, and caused a lack of actin stress fibers and the appearance of F-actin rich membrane ruffles (Fig. 7A). At 120 min, in wild-type MEFs, the actin stress fibers were notably increased and co-localized with vinculin at the end of these fibers at focal adhesion sites. Furthermore, the morphology also changed to that of fibroblasts. In contrast, few stress fibers and morphological changes were observed in *fad104*$^{-/-}$ MEFs. In addition, vinculin in *fad104*$^{-/-}$ MEFs was not distributed to focal adhesion sites, and not co-localized with actin stress fibers (Fig. 7A). After 480 min, *fad104*$^{-/-}$ MEFs had spread more than was observed at 120 min, and developed actin stress fibers with vinculin at their ends, but were still less well spread than wild-type MEFs (Fig. 7A). These results indicated that the disruption of *fad104* reduced the numbers of stress fibers formed and cell adhesion sites, and delayed the change in cell morphology and cell spreading.

To test whether *fad104* regulates cell adhesion, we further performed a quantitative cell adhesion assay by counting the attached cells in the tissue culture. Wild-type and *fad104*$^{-/-}$ MEFs were plated onto fibronectin-coated plates. The attached cells

Author's personal copy

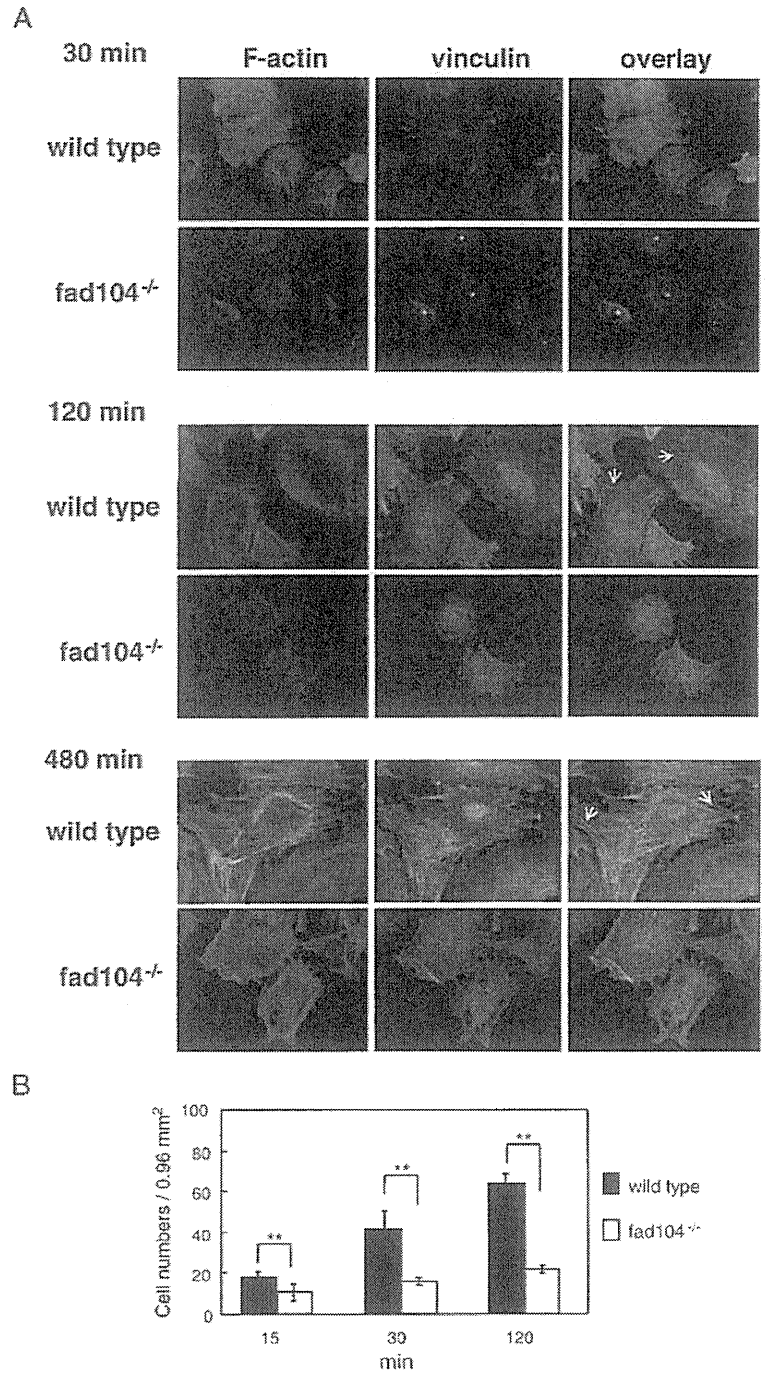

Fig. 7 – Deletion of *fad104* causes delayed stress fiber formation, cell adhesion and cell spreading. (A) Immunofluorescence of wild-type and *fad104*$^{-/-}$ MEFs. MEFs (4×10^4) from wild-type and *fad104*$^{-/-}$ embryos were plated on fibronectin-coated (3 μg/ml) cell disks in 24-well plates. At 30, 120 and 480 min from seeding, F-actin and vinculin were visualized with TRITC-conjugated phalloidin (red) and anti-vinculin antibody (green), respectively. Overlay demonstrates that the end of stress fibers co-localizes with vinculin (yellow). The arrow shows the typical end of stress fibers. A representative field at each time point is shown. (B) Cell adhesion assay of wild-type and *fad104*$^{-/-}$ MEFs. MEFs (1×10^4) from wild-type and *fad104*$^{-/-}$ embryos were plated onto fibronectin-coated (3 μg/ml) 24-well plates. At each time point, the attached cells were photographed, and counted in five random microscopic fields per plate. The data represent means with standard deviations ($n=5$). $^{**}p<0.01$.

Author's personal copy

were photographed and counted at 15, 30 and 120 min after plating. At all time points, the *fad104*$^{-/-}$ MEFs dramatically showed impaired adhesion compared with the wild-type MEFs (Fig. 7B). The results in Figs. 7A and B strongly suggest that *fad104* is a novel factor involved in cell adhesion and spreading.

Disruption of fad104 inhibited cell migration

Finally, we examined the effects of disruption of *fad104* on cell migration. The ability of cells to migrate was evaluated with a wound healing assay. The confluent monolayers of wild-type and *fad104*$^{-/-}$ MEFs were wounded with a yellow tip. The damaged area was photographed and measured at the time of wounding. The wound of wild-type MEFs gradually healed and was almost closed after 10 h. On the other hand, wound closure for *fad104*$^{-/-}$ MEFs was remarkably delayed, and the wound was not completely closed within 10 h (Fig. 8A). The area of the wound that was not covered by migrating cells within 10 h was measured by NIH-Image J software (Fig. 8B). At all time points, the wound closure of *fad104*$^{-/-}$ MEFs was notably and significantly repressed compared to that of wild-type MEFs. Even after 10 h, almost half the area was still uncovered in *fad104*$^{-/-}$ MEFs. These results indicate that *fad104* is necessary for cell migration.

Discussion

The molecular mechanism of adipocyte differentiation is very complex. Previous studies indicated that transcription factors including PPARγ, the C/EBP family and SREBP-1 regulated the differentiation process. MEFs prepared from PPARγ-deficient mice failed to differentiate into adipocytes [25]. Furthermore, the double knockout of C/EBPβ and C/EBPδ impaired the synthesis of fat in mice [24]. SREBP-1 is known to be required for production of ligands of PPARγ [26]. However, these three families of transcription factors are expressed at the middle and late stages of adipogenesis. On the other hand, it is not clear which factors regulate adipocyte differentiation at the initial stage.

Previously, we identified many genes that were expressed early on in the differentiation of 3T3-L1 cells into adipocytes [4,5]. *fad104* is a novel gene included among the isolated genes. Since knockdown of its expression inhibited the differentiation process, *fad104* has indispensable roles in the differentiation of 3T3-L1 preadipocytes. However, little was known about the functions and physiological roles of *fad104*.

In this study, to examine the actual biological functions of *fad104*, we generated mice with a homozygous null *fad104*

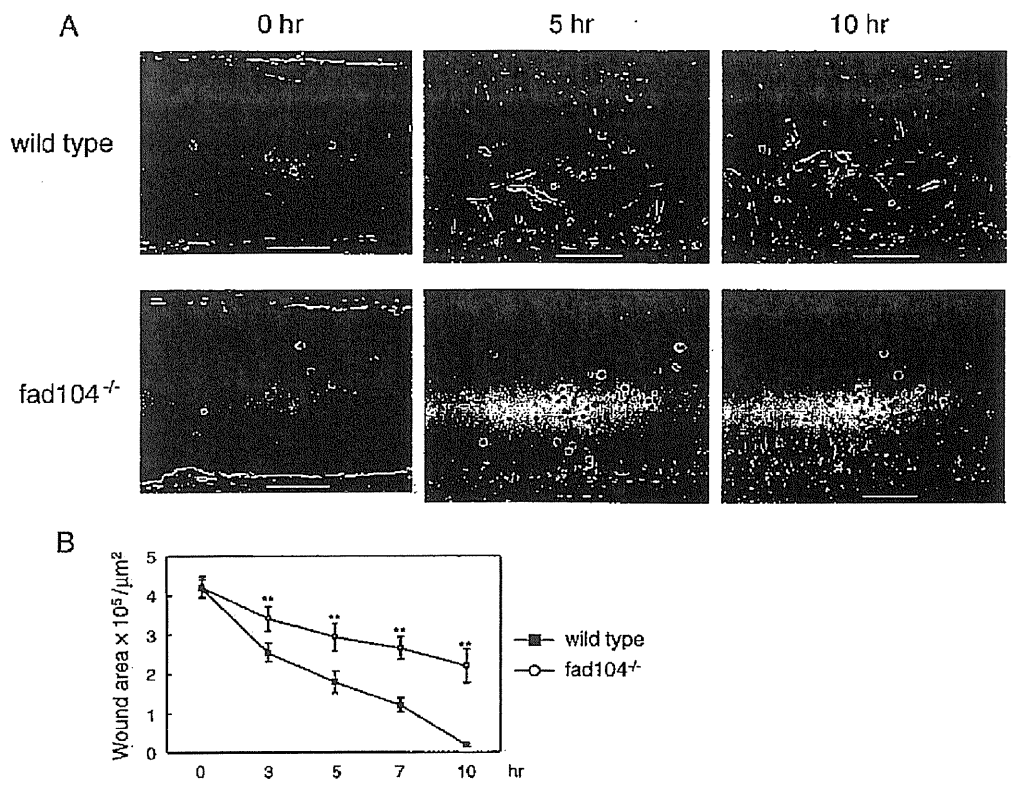

Fig. 8 – Disruption of *fad104* inhibits cell migration in wound healing assay. (A) Wound healing assay of wild-type (top panels) and *fad104*$^{-/-}$ MEFs (bottom panels). MEFs were plated and grown to confluence. At 1 day postconfluence, a wound was introduced into the monolayer, and the migration of cells was monitored using photographs taken at time points from 0 to 10 h. The 0, 5 and 10 h time points are shown for each cell line. (B) Quantification of the wound healing assay shown in panel A. For each cell line, the wound area was quantified by using NIH-Image J software. The data represent means with standard deviations (n=4). **$p<0.01$.

Author's personal copy

mutation. Interestingly, the *fad104*-deficient mice died within 1 day of birth. All of the *fad104*-deficient pups at E18.5 were breathing and moving just after caesarean section, suggesting that the disruption of *fad104* caused rapid postnatal death. It is well known that the maintenance of blood glucose levels and the thermoregulation have pivotal roles for survival of newborn pups just after birth [27,28]. However, as shown Fig. 2, *fad104*-deficient neonates did not exhibit the abnormalities about blood glucose level, body temperature, and BAT weight. In our previous reports, *fad104* was found to be highly expressed in white adipose tissue (WAT). On the other hand, *fad104* was also modestly expressed in heart, kidney and lung [12]. Since little WAT is found in newborns, it is possible that the postnatal lethality observed in *fad104*-deficient mice is caused by a functional disorder of *fad104* in organs including the heart, kidney and lung. In order to elucidate the cause of the rapid death after birth of *fad104*-deficient mice, a pathological analysis of these organs is now ongoing.

Kuma et al. indicated that mice deficient for *Atg5*, which is essential for autophagosome formation, die within 1 day at birth, suggesting that autophagic degradation of proteins is important for survival during neonatal starvation [29]. We attempted to examine whether *fad104* is involved in the regulation of autophagic activity. During autophagy, microtubule-associated protein light chain (LC3) is processed from the cytosolic form, LC3-I, to the membrane-bound form, LC3-II. Since the amount of LC3-II correlates with the number of autophagosomes, immnoblotting of endogenous LC3 can be used to measure autophagic activity. Therefore, we performed Western blotting analysis using the cell lysates prepared from wild-type and *fad104*$^{-/-}$ MEFs under nutrition starvation. Commercially available anti-LC3 antibody, which was employed the detection of endogenous LC3 in MEFs was used [30]. However, we could detect neither LC3-I nor LC3-II in the cell lysates prepared from wild-type and *fad104*$^{-/-}$ MEFs, whereas both LC3-I and LC3-II proteins were detected in the cell lysate prepared from HeLa cells under starvation condition as described previously [31]. Although we could not conclude whether *fad104* is related to autophagic activity in this study, it is necessary to elucidate the relationship between *fad104* and autophagic activity by further analyses.

Although it is well known that the proteins containing the fibronectin type III domain localize to the cell surface, the FAD104 localized to the ER, but not the plasma membrane. Therefore, FAD104 may be a novel protein localized to the ER. The proteins found in the ER have an important role of various cellular functions. For example, calreticulin, a Ca^{2+}-binding protein of the ER, influences the cell spread and cell adhesion via the regulation of c-Src activities and vinculin expression [32,33]. Therefore, we next examined whether a novel gene, *fad104*, also is involved in various cellular functions. Analyses of MEFs prepared from *fad104*-deficient mice demonstrated *fad104* to be crucial for cell proliferation, adhesion, spreading and migration.

As shown in Fig. 6, the disruption of *fad104* caused the reduction of the increase of the cell numbers during 6 days after seeding. This result indicates that the proliferation rate of *fad104*$^{-/-}$ MEFs was slightly attenuated than that of wild-type MEFs. *Fad104*-deficient MEFs also exhibited a delay in cell adhesion and cell spreading (Fig. 7). It is necessary to explore the mechanism which *fad104* regulates the cell proliferation.

Cell migration, cell spreading and adhesive properties are regulated by continuous remodeling of the actin cytoskeleton. For example, in cell migration, the actin structures are divided into three steps; the lamelipodial actin network at the leading edge of the cell, filopodial bundles beneath the plasma membrane, and contractile actin stress fibers in the cytoplasm [34]. At the early stage of adipocyte differentiation, the change to the actin organization is very important. Kawaguchi et al. indicated that ADAM12, a disintegrin and metalloprotease, altered the organization of the actin cytoskeleton and extracellular matrix by impairing the function of β1 integrin, and induced differentiation into mature adipocytes [35]. A deficiency of *fad104* dramatically reduces the formation of stress fibers, strongly suggesting that *fad104* also functions as a key regulator of the actin cytoskeleton's organization, and may promote adipogenesis in the early stages of the differentiation process.

Recently, Obholz et al. reported that a fibronectin type III domain containing 3a (FNDC3A) is necessary for adhesion between spermatids and Sertoli cells, and the mutation of *fndc3a* is the cause of male sterility in symplastic spermatids (sys) mice [36]. FNDC3a is closely related to FAD104, since FNDC3a also contains 9 repeats of the fibronectin type III domain and transmembrane domain. It is of interest that FNDC3a is also necessary for mediating adhesion during spermatogenesis. However, FNDC3a does not have a RGD tripeptide sequence in any fibronectin type III domain repeat sequence. In addition, the disruption of FNDC3a does not cause postnatal death. Thus, although FAD104 and FNDC3a are very similar, these two proteins might have distinct and different roles in cellular functions and developmental processes.

In summary, the present study provided some new insights into the functions of a novel gene, *fad104*, namely as essential for the survival of newborns just after birth and as important for cell proliferation, adhesion, spreading and migration. Although further investigation is definitely needed, *fad104* may play an important role in the late stage of embryonic development or neonates after birth via the regulation of cell proliferation, adhesion, spreading and migration. Furthermore, it is possible that *fad104* regulates these cellular functions by altering the actin cytoskeleton's organization. Although we have no information on how *fad104* regulates the survival of neonates or adipocyte differentiation yet, further analyses of *fad104* would help us to understand not only the signaling pathways at the early stage of adipocyte differentiation but also the molecular mechanisms of survival after birth.

Acknowledgments

We thank Dr. Kei Tominaga and Chiharu Kondo for the construction of targeting vectors and screening of positive ES clones. We are grateful to Misaki Fujimura for the construction of fad104 expression plasmid. We also thank Dr. Takashi Ueda for histological analyses. This work was supported in part by grants from the Ministry of Education, Culture, Sports, Science and Technology (MEXT), Japan, Japan Society for the Promotion of Science (JSPS), the grant-in-aid for research in Nagoya City University, and the Takeda Science Foundation.

REFERENCES

[1] P.G. Kopelman, Obesity as a medical problem, Nature 404 (2000) 635–643.
[2] R.P. Brun, J.B. Kim, E. Hu, S. Altiok, B.M. Spiegelman, Adipocyte differentiation: a transcriptional regulatory cascade, Curr. Opin. Cell Biol. 8 (1996) 826–832.

Author's personal copy

[3] E.D. Rosen, C.J. Walkey, P. Puigserver, B.M. Spiegelman, Transcriptional regulation of adipogenesis, Genes Dev. 14 (2000) 1293–1307.
[4] M. Imagawa, T. Tsuchiya, T. Nishihara, Identification of inducible genes at the early stage of adipocyte differentiation of 3T3-L1 cells, Biochem. Biophys. Res. Commun. 254 (1999) 299–305.
[5] M. Nishizuka, T. Tsuchiya, T. Nishihara, M. Imagawa, Induction of Bach1 and ARA70 gene expression at an early stage of adipocyte differentiation of mouse 3T3-L1 cells, Biochem. J. 361 (2002) 629–633.
[6] M. Nishizuka, K. Honda, T. Tsuchiya, T. Nishihara, M. Imagawa, RGS2 promotes adipocyte differentiation in the presence of ligand for peroxisome proliferator-activated receptor gamma, J. Biol. Chem. 276 (2001) 29625–29627.
[7] M. Nishizuka, E. Arimoto, T. Tsuchiya, T. Nishihara, M. Imagawa, Crucial role of TCL/TC10beta L, a subfamily of Rho GTPase, in adipocyte differentiation, J. Biol. Chem. 278 (2003) 15279–15284.
[8] A. Kitamura, M. Nishizuka, K. Tominaga, T. Tsuchiya, T. Nishihara, M. Imagawa, Expression of p68 RNA helicase is closely related to the early stage of adipocyte differentiation of mouse 3T3-L1 cells, Biochem. Biophys. Res. Commun. 287 (2001) 435–439.
[9] K. Tominaga, Y. Johmura, M. Nishizuka, M. Imagawa, Fad24, a mammalian homolog of Noc3p, is a positive regulator in adipocyte differentiation, J. Cell. Sci. 117 (2004) 6217–6226.
[10] K. Tominaga, T. Kagata, Y. Johmura, T. Hishida, M. Nishizuka, M. Imagawa, SLC39A14, a LZT protein, is induced in adipogenesis and transports zinc, FEBS J. 272 (2005) 1590–1599.
[11] K. Tominaga, C. Kondo, T. Kagata, T. Hishida, M. Nishizuka, M. Imagawa, The novel gene fad158, having a transmembrane domain and leucine-rich repeat, stimulates adipocyte differentiation, J. Biol. Chem. 279 (2004) 34840–34848.
[12] K. Tominaga, C. Kondo, Y. Johmura, M. Nishizuka, M. Imagawa, The novel gene fad104, containing a fibronectin type III domain, has a significant role in adipogenesis, FEBS Lett. 577 (2004) 49–54.
[13] Y. Johmura, S. Osada, M. Nishizuka, M. Imagawa, FAD24 acts in concert with histone acetyltransferase HBO1 to promote adipogenesis by controlling DNA replication, J. Biol. Chem. 283 (2008) 2265–2274.
[14] D. Craig, M. Gao, K. Schulten, V. Vogel, Structural insights into how the MIDAS ion stabilizes integrin binding to an RGD peptide under force, Structure 12 (2004) 21–30.
[15] R. Pankov, K.M. Yamada, Fibronectin at a glance, J. Cell. Sci. 115 (2002) 3861–3863.
[16] S.K. Sastry, K. Burridge, Focal adhesions: a nexus for intracellular signaling and cytoskeletal dynamics, Exp. Cell Res. 262 (2000) 25–36.
[17] B.H. Geiger, A. Bershadsky, R. Pankov, K.M. Yamada, Transmembrane crosstalk between the extracellular matrix–cytoskeleton crosstalk, Nat. Rev. Mol. Cell Biol. 2 (2002) 793–805.
[18] R.D. Bowditch, M. Hariharan, E.F. Tominna, J.W. Smith, K.M. Yamada, E.D. Getzoff, M.H. Ginsberg, Identification of a novel integrin binding site in fibronectin. Differential utilization by beta 3 integrins, J. Biol. Chem. 269 (1994) 10856–10863.
[19] T. Nagai, N. Yamakawa, S. Aota, S.S. Yamada, S.K. Akiyama, K. Olden, K.M. Yamada, Monoclonal antibody characterization of two distant sites required for function of the central cell-binding domain of fibronectin in cell adhesion, cell migration, and matrix assembly, J. Cell Biol. 114 (1991) 1295–1305.
[20] B.M. Spiegelman, S.D. Farmer, Decreases in tubulin and actin gene expression prior to morphological differentiation of 3T3 adipocytes, Cell 29 (1982) 53–60.
[21] B.M. Spiegelman, C.A. Ginty, Fibronectin modulation of cell shape and lipogenic gene expression in 3T3-adipocytes, Cell 35 (1983) 657–666.
[22] L. Yang, L. Wang, Y. Zheng, Gene targeting of Cdc42 and Cdc42GAP affirms the critical involvement of Cdc42 in filopodia induction, directed migration, and proliferation in primary mouse embryonic fibroblasts, Mol. Biol. Cell 17 (2006) 4675–4685.
[23] F. Chen, Y. Lu, V. Castranova, Z. Li, M. Karin, Loss of IKKβ promotes migration and proliferation of mouse embryo fibroblast cells, J. Biol. Chem. 281 (2006) 37142–37149.
[24] T. Tanaka, N. Yoshida, T. Kishimoto, S. Akira, Defective adipocyte differentiation in mice lacking the C/EBPbeta and/or C/EBPdelta gene, EMBO J. 16 (1997) 7432–7443.
[25] N. Kubota, Y. Terauchi, H. Miki, H. Tamemoto, T. Yamauchi, K. Komeda, S. Satoh, R. Nakano, C. Ishii, T. Sugiyama, K. Eto, Y. Tsubamoto, A. Okuno, K. Murakami, H. Sekihara, G. Hasegawa, M. Naito, Y. Toyoshima, S. Tanaka, K. Shiota, T. Kitamura, T. Fujita, O. Ezaki, S. Aizawa, R. Nagai, K. Tobe, S. Kimura, T. Kadowaki, PPAR gamma mediates high-fat diet-induced adipocyte hypertrophy and insulin resistance, Mol. Cell 4 (1999) 597–609.
[26] J.B. Kim, B.M. Spiegelman, ADD1/SREBP1 promotes adipocyte differentiation and gene expression linked to fatty acid metabolism, Genes Dev. 10 (1996) 1096–1107.
[27] B. Cannon, J. Nedergaard, Brown adipose tissue: function and physiological significance, Physiol. Rev. 84 (2004) 277–359.
[28] M.E. Symonds, M.A. Lomax, Material and environmental influences on thermoregulation in the neonate, Proc. Nutr. Soc. 51 (1992) 165–172.
[29] A. Kuma, M. Hatano, M. Matsui, A. Yamamoto, H. Nakaya, T. Yoshimori, Y. Ohsumi, T. Tokuhisa, N. Mizushima, The role of autophagy during the early neonatal starvation period, Nature 432 (2004) 1032–1035.
[30] C.P. Cheng, M.C. Yang, H.S. Liu, Y.S. Lin, H.Y. Lei, Concanavalin A induces autophagy in hepatoma cells and has a therapeutic effect in a murine in situ hepatoma model, Hepatology 45 (2007) 286–296.
[31] Y. Kabeya, N. Mizushima, T. Ueno, A. Yamamoto, T. Kirisako, T. Noda, E. Kominami, Y. Ohsumi, T. Yoshimori, LC3, a mammalian homologue of yeast Apg8p, is localized in autophagosome membranes after processing, EMBO J. 19 (2000) 5720–5728.
[32] S. Papp, M.P. Fadel, H. Kim, C.A. McCulloch, M. Opas, Calreticulin affects fibronectin-based cell-substratum adhesion via the regulation of c-Src activity, J. Biol. Chem. 282 (2007) 16585–16598.
[33] M. Opas, M.S. Pawlikowski, G.K. Jass, N. Mesaeli, M. Michalak, Calreticulin modulates cell adhesiveness via regulation of vinculin expression, J. Cell Biol. 135 (1996) 1913–1923.
[34] P. Hatulainen, P. Lappalainen, Stress fibers are generated by two distinct actin assembly mechanisms in motile cells, J. Cell Biol. 173 (2006) 383–394.
[35] N. Kawaguchi, C. Sundberg, M. Kveiborg, B. Moghadaszadeh, M. Asmar, N. Dietrich, C.K. Thodeti, F.C. Nielson, P. Moller, A.M. Mercurio, R. Albrechtsen, U.M. Wewer, ADAM12 induces actin cytoskeleton and extracellular matrix reorganization during early adipocyte differentiation by regulating beta1 integrin function, J. Cell. Sci. 116 (2003) 3893–3904.
[36] K.L. Obholz, A. Akopyan, K.G. Waymire, G.R. MacGregor, FNDC3A is required for adhesion between spermatids and Sertoli cells, Dev. Biol. 298 (2006) 498–513.